

4282

**LARGE SCALE MONTE CARLO SIMULATION
OF CROSSFLOW MEMBRANE FILTRATION FOR
REMOVAL OF PARTICULATE MATERIALS**

**A THESIS SUBMITTED TO THE GRADUATE DIVISION OF THE
UNIVERSITY OF HAWAII IN PARTIAL FULFILMENT OF THE
REQUIREMENTS FOR THE DEGREE OF**

MASTER OF SCIENCE

IN

CIVIL ENGINEERING

MAY 2008

BY

Yuewei Liu

Thesis Committee:

Albert S. Kim, Chairperson

Clark C.K. Liu

Michelle H. Teng

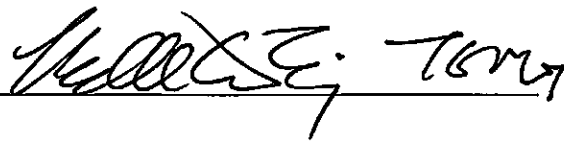
4282

We verify that we have read this thesis and that, in our opinion, it is satisfactory in scope and quality as a thesis for the degree of Master of Science in Civil Engineering.

THESIS COMMITTEE


Chairperson





ACKNOWLEDGEMENTS

I would like to express my deep and sincere gratitude to my advisor, Dr. Albert S. Kim, professor of Civil and Environmental Engineering, University of Hawaii. His wide knowledge and logical way of thinking have been of great value for me. I appreciate his great assistance in writing reports, including the seminar abstract, proposal, project report for the grants from the Maui High Performance Computing Center and National Science Foundation, and also this thesis. His understanding, encouraging, and patient guidance have provided a good basis for my thesis and future career. I am deeply grateful to my advisor for his great support throughout my two years of study at the University of Hawaii. I also wish to express my warm and sincere thanks to Drs. Clark C.K. Liu and Michelle H. Teng, professors of Civil and Environmental Engineering, University of Hawaii, for their precious comments and valuable suggestions.

I would also like to thank my family for the support they provided to me throughout my entire life. I especially give my loving thanks to my husband Xin Zhang, my daughter Chuheng Zhang, and my son Chufeng Zhang. Without their encouragement and understanding, it would have been impossible for me to finish this thesis.

ABSTRACT

Membrane separation has emerged as a cost competitive, viable, and alternative way to achieve high quality effluent in comparison to conventional methods for drinking and industrial water production and also water reuse. However, membrane fouling, caused by deposition of suspended and dissolved solids, results in decreased performance of the filtration, especially a decline in permeate flux through the membrane. Membrane fouling can be minimized by chemical modification of the membrane surface, periodic backwashing/cleaning, and optimum operational conditions. Critical flux, which is defined as the flux below which no fouling occurs, is becoming a crucially important concept related to optimum operation. Several methods were used to experimentally measure the critical flux, including direct observation through membrane, mass balance, and flux-pressure observations.

In this study, a large-scale Monte Carlo simulation method for crossflow membrane filtration to remove particulate materials is developed to investigate dynamic particle structures associated with the critical flux. This computational study is performed on a parallel computer platform via message passing interface (MPI). Dominant mechanisms of particle transport, including Brownian and shear-induced diffusion, are incorporated

and unified into an effective hydrodynamic force acting on hard spheres in the concentrated shear flow. Biased probability distribution, including tangential and normal biases, is used in the Monte Carlo simulations.

Critical fluxes are first visually estimated by observing particle configurations, and they are in a good agreement with experimental observations done by multiple researchers with various operational conditions. Effects of shear rate and particle size on the critical flux are also investigated using this force-biased Monte Carlo simulation method, which shows that repulsive particles lead to higher critical flux compared to that of hard sphere particles. Variance of the particle distribution is proposed to be an order parameter, and its second order derivative is used to estimate the critical flux. The simulated critical fluxes are in good agreement with those of experimental results using the particle mass balance method.

TABLE OF CONTENTS

	Page
ACKNOWLEDGEMENTS.....	i
ABSTRACT.....	ii
TABLE OF CONTENTS.....	iv
LIST OF FIGURES.....	vi
CHAPTER 1. INTRODUCTION.....	1
CHAPTER 2. LITERATURE REVIEW.....	10
2.1 Classification of Membrane Filtration.....	10
2.2 Concentration Polarization and Membrane Fouling.....	13
2.3 Permeate Flux.....	18
2.4 Critical Flux.....	22
2.4.1 Direct Observation through the Membrane.....	23
2.4.2 Mass Balance.....	24
2.4.3 Flux-Pressure Observation.....	25
2.5 Constant Transmembrane Pressure and Constant Flux Modes.....	26
2.6 Membrane Filtration Simulation.....	29
2.6.1 Conventional Mathematical Model.....	29

2.6.2 Monte Carlo Simulation.....	35
CHAPTER 3. SIMULATION METHOD.....	40
3.1 Ambient Flow Field.....	40
3.2 Modeling System.....	41
3.3 Biased Probability Distribution.....	44
3.3.1 Tangential Bias.....	44
3.3.2 Normal Bias.....	47
3.4 Parallel Algorithm.....	48
3.4.1 Domain Dcomposition.....	48
3.4.2 Communications among Processors.....	49
3.5 Initialization of Simulation.....	50
3.5.1 Dimension of Membrane Channel.....	50
3.5.2 Initial Volume Fraction.....	50
3.5.3 Boundary Condition.....	51
CHAPTER 4. RESULTS AND DISCUSSION.....	52
4.1 Verification of Mechanisms.....	52
4.2 Order Parameter.....	55
4.3 Critical Flux.....	60
CHAPTER 5. CONCLUSIONS.....	64
REFERENCES.....	82

LIST OF FIGURES

FIGURE	Page
1.1 Diagram for a typical water treatment plant.....	66
1.2 Conceptual illustration of dead-end filtration.....	67
1.3 Conceptual illustration of crossflow filtration.....	68
2.1 Diagram of membrane filtration process.....	69
2.2 Diagram of membrane filtration processes (MF, UF, NF, and RO).....	70
3.1 Flow lines in the upper half of membrane channel (Berman, 1953).....	71
3.2 The simulation box as a representative volume.....	72
3.3 Dominant transport mechanisms at different locations within the membrane channel.....	73
3.4 Domain decomposition among four processors along x -direction.....	74
3.5 Diagram of master-slave parallel algorithm and MPI as shown in Figure 3.4.....	75
4.1 Canonical MC simulations with the number of particles $N_p = 2100$, particle radius $a = 0.1\mu m$, mass density $\rho_p = \rho_f$, and shear rate $\dot{\gamma} = 10^3 \text{ sec}^{-1}$. The permeate flux v_w of simulations are (a) $0\mu m$, (b) $1\mu m$, (c) $5\mu m$, (d) $10\mu m$, (e) $20\mu m$, and (f) $30\mu m$	76

4.2 Profiles of particle volume fraction in the normal direction with various permeate fluxes with (a) linear and (b) common-log scales of volume fraction. Particle radius is $0.1 \mu m$, and shear rate is 1000 sec^{-1}	77
4.3 Profiles of particle volume fraction in the normal direction with various permeate flux with (a) linear and (b) common-log scales of volume fraction.....	78
4.4 The order parameter defined as Eq. (4.1) versus the permeate flux.....	79
4.5 The derivative of the order parameter with respect to the permeate flux, obtained from Fig 4.4.....	80
4.6 Comparison of critical fluxes determined from MC simulation method and those from experimental observations.....	81

CHAPTER 1. INTRODUCTION

A shortage of water due to an ever increasing world population and intensified demands for agriculture and industry has resulted in wastewater reuse becoming a primary source of potable water. Consequently, quality as well as quantity of treated water is one of the most serious public concerns.

The removal of particulate matters, a crucial step in water and wastewater treatment, is complicated by the diverse nature of particles, which range from inorganic minerals and debris to agglomerates of complex organic substances. For instance, the mass of outfall particulates discharged annually into the ocean by the five major southern California municipal waste systems is about 2.9×10^5 metric tons, dry weight. At a compaction density of 1g/cm^3 without void volume, material of this volume would constitute a 1mm thick blanket if it were spread over the sea-bottom (Kavanaugh and Leckie, 1980).

Apart from suspended matters, many other contaminants are associated with particles. For example, the attachment of microorganisms such as bacteria to suspended

particulates tends to support long bacterial survival because the nutrients, which are already absorbed by the particulates, are readily available for bacterial uptake. Parel (Parel, 1975) found the levels of nutrients to be 10 to 100 times higher on the particulate surface than in the surrounding water column. Although particulate matter in the form of biomass is a necessary prerequisite in many water treatment schemes, particles always represent undesired pollutants in most product waters, and the removal of all particulate materials is the main goal for water and wastewater treatment.

Currently, both conventional treatment and membrane systems are being used for particulate matter removal from water and wastewater. Conventional treatment plants typically consist of coagulation, flocculation, sedimentation, filtration, and disinfection. Figure 1.1 shows a process diagram for a typical water treatment plant. Although conventional treatment systems outlined in Figure 1.1 can be used to provide good quality potable water, the granular media filters represent a probabilistic rather than an absolute barrier; consequently, pathogens can still pass through the filters and pose a health risk. Driven by the need to protect public health from water borne pathogens, the Environmental Protection Agency (EPA) has progressively developed regulations that require higher standards for treated water quality to prevent the passage of infectious pathogens into the drinking water supply. Conventional treatment processes, however,

cannot provide sufficient quality of effluent for unrestricted use and meet stringent EPA standard.

Compared to conventional treatment, membrane filtration is a promising alternative technology. A membrane is an interface between two phases and is capable of separating species as a function of their physical and chemical properties when a driving force is applied across it. A membrane is generally described as a selective material barrier that readily allows solvent transport but efficiently rejects solutes (Mulder, 1996). In clean water production, the solvent is water and solutes are any undesirable materials that need to be removed.

Membrane filtration is a term used to describe the removal of particulates from feedwater. Microfiltration (MF) and Ultrafiltration (UF) are the two processes that are most often associated with the term “membrane filtration.” MF and UF are characterized by their ability to remove suspended or colloidal particles via a sieving mechanism based on the size of the membrane pores relative to that of the particulate matter.

The interest in using MF or UF as pretreatment to reverse osmosis (RO), a filtration process that can remove everything, for high-fouling feed water processing dates back to the 1980's. However, the MF/UF design was generally dismissed as a commercial alternative or supplement to conventional processes due to capital costs.

Over the last couple of years, membrane alternatives have drawn increasing interest and undergone significant advances, and the use of MF/UF as a water filtration process has exploded in the municipal market place. There are several hundred MF/UF systems in operation in municipal drinking water systems throughout the world, with total capacities exceeding 200 million gallons per day (MGD) (Bergman, 1999). Drivers for this advance include not only desalination to combat water scarcity but also the removal of various materials from water to comply with increasingly stringent environmental legislation such as Giardia and Cryptosporidium removal guidelines for US Surface Water Treatment Rule. Innovations in membrane manufacturing and process conditions have led to a dramatic decrease in membrane filtration costs, including capital and operating costs.

Consequently, membrane filtration has emerged as a cost-competitive, viable alternate to achieve high quality effluent compared to conventional methods in drinking and industrial water production and also in recycling and reuse. Membranes also have the advantage of a small footprint for a processing plant. In other words, the required space will be considerably reduced after replacing the flocculation and sedimentation basins, and granular media filter shown in Figure 1.1 by one membrane filtration unit. Also, potential water quality benefits arise because the membranes may block a substantial fraction of the small colloids, low molecular weight natural organic matters (NOM), and

microorganisms that do not settle and pass through conventional sand filters. Besides, membranes have the advantage of reducing chemical requirements since they retain even small flocs. In this way, membrane systems provide an effluent that can be more easily disinfected and is less likely to produce undesirable disinfection by-products (DBPs).

However, as a result of the accumulation of particles on the membrane as it removes suspended solids, a particle deposit layer called a cake layer will form on the membrane surface. Membrane fouling, caused by the deposition of suspended or dissolved solids on the external membrane surface, at the membrane pores, or within the membrane pores, results in decreased performance.

Particle deposition, biofouling and scaling are three main types of membrane fouling. Pore blocking is a phenomenon wherein particles block pores on the membrane surface, while pore plugging refers to pore constriction or solute adsorption on the pore walls. Resistance as a consequence of transport, adsorption, and growth of biocolloids is called biofouling. Fouling exerts severe limitations to the future growth of membrane technology. Scaling, occurring mainly in reverse osmosis (RO) and nanofiltration (NF), refers to the deposition of "hard scale" on the membrane due to the concentration of sparingly soluble salts (such as BaSO_4 and MgCl_2) that exceed the solubility limit. Particulate fouling is an especially persistent problem in all membrane filtration

processes, and refers to the deposition of suspended matter, colloids, and microorganisms on the membrane surface.

Problems arising from membrane fouling are the main reasons for reduction in product water flux or increasing operational pressures to maintain flux, which translates into increased operational costs. Membrane cleaning to remove fouling particulate matter results in frequent down time and increased energy and chemical use. Wastewater from membrane cleaning also adds additional costs.

It is widely recognized that control of particulate fouling is instrumental in further membrane technology advancement and in decreasing costs associated with this process. This can only be achieved when fouling mechanisms of feed water are well characterized and understood. To understand fouling mechanisms, a pilot plant operation is commonly used prior to designing and installing full-scale systems. Although this method generally provides a reasonable way to predict particulate fouling in membrane filtration systems, it is time consuming, expensive, and sometimes does not represent performance of full-scale systems.

Compared to pilot plant operations or experimental approaches, computer modeling is fast and cost-effective. In addition, it provides a better scientific understanding with the ability to include practical complications. Due to the availability

of faster computers, especially supercomputers and PC clusters, it is possible to build a full-scale model of particle transport at a precise microscopic level, which is capable of discretely computing each particle displacement individually. The classic methods for undertaking rigorous modeling include Brownian Dynamics (Ermak, 1975; Ermak and Buckholtz, 1980; Van Gusteren and Berendsen, 1982; Allen, 1980), Molecular Dynamics (Verlet, 1967) and Monte Carlo Simulation (Allen and Tildesley, 1987; Manousiouthakis and Deem, 1999; Metropolis, et al., 1953). Chen and Kim (Chen and Kim, 2004) provided a copious review of the literature on the attributes of these methods.

Membrane filtration systems can be classified into dead-end filtration and crossflow filtration. Membrane filtration systems operating in dead-end mode utilizing no concentrate stream such that there is only one influent and one effluent stream, as shown in Figure 1.2, are also called “normal” or “direct” filtration systems. In the dead-end mode of operation, contaminants suspended in the feed stream accumulate on the membrane surface and are held in place by hydraulic forces acting normal to the membrane, forming a cake layer. However, if a scouring force using water and/or air is applied parallel to the membrane surface during filtration in a continuous or intermittent manner, as illustrated in Figure 1.3, the systems are called crossflow filtration systems. Belfort et al. (Belfort et al., 1994) gave a rigorous review about crossflow microfiltration.

Compared to dead-end mode filtration, the accumulation of contaminants at the surface of the membrane in crossflow filtration is significantly reduced, hence, membrane fouling will be relieved to some extent. The crossflow model is a typical configuration in membrane filtration. In crossflow filtration the solution is pumped to flow tangentially over the membrane surface. The objective of crossflow filtration is to maintain a high scouring velocity across the membrane surface to minimize particle deposition and membrane fouling. Crossflow membrane processes operate in an unsteady-state manner in which suspended solids accumulate on the feed side of membrane over the course of filtration cycle, which means that the membrane must be cleaned before it reaches a steady state with minute permeate flux.

For crossflow filtration processes, there are two known modes of operation-constant transmembrane pressure (TMP) operation and constant flux operation. In constant TMP mode, TMP is maintained constant throughout the filtration run, and hence, permeate flux decreases with time due to concentration polarization followed by membrane fouling. In the constant flux mode, in order to maintain a constant permeate flux, TMP becomes a transient variable.

The goal of this study is to develop a Monte Carlo simulation model using constant permeate flux mode to find optimum operation conditions, i.e. the optimum

permeate flux. Then this model can be extended to a large-scale model to simulate the real scenario of crossflow membrane filtration for particulate matters removal. In order to present the full-scale scenario of filtration, a large number of calculations are needed, so the model is built on a platform of parallel computing via Message Passing Interface (MPI).

CHAPTER 2. LITERATURE REVIEW

The principle of membrane filtration is shown in Figure 2.1. The membrane acts as a very specific filter, which has the capability of allowing the passage of water more readily than any solutes. When feed water is pressurized into the membrane channel, water flows through and solutes will not. The water passing through the membrane forms the permeate flow, which is clean and drinkable, meeting potable water regulations.

There are various methods enable substances to penetrate a membrane. For example, pressure difference, temperature difference, concentration difference, voltage and so on. If pressure is applied, most commonly used in water and wastewater filtration, it is called pressure driven membrane filtration.

2.1 Classification of Membrane Filtration

Pressure-driven membrane processes for water treatment are classified into four categories by the size-range of materials separated (AWWAR, 1996). These categories are microfiltration (MF), ultrafiltration (UF), nanofiltration (NF), and reverse osmosis

(RO). Each membrane functions as a filter for solute matters of various sizes. Figure 2.2 shows the schematic representation of MF, UF, NF and RO membrane filtration processes.

MF membranes have the largest pores, ranging from $0.1 \mu m$ to $10 \mu m$, and the highest permeability, so that a sufficient water flux is obtained at a low pressure. Components larger than the pore size are removed by a sieving mechanism. The smallest pore sizes correspond to the size of suspended solids, colloids, and bacteria, which are retained by a sieving mechanism (Bruggen et al., 2003). Germs and viruses are not removed. There is, however, quite a gap between real practice and this ideal situation. MF is a process in which suspended colloids and particles in the approximate size range 0.1 to $20 \mu m$ are retained by microporous membranes. MF is usually operated at relatively low transmembrane pressures (<50 psi or 3.5 Mpa) and very high permeation fluxes ($10^{-4} - 10^{-2} m/s$ for unfouled membranes) (Zeman and Zydney, 1996), and it is these factors that distinguish MF from both RO and UF.

UF membranes have smaller pores (2 to 100 nm), and the permeability is considerably lower than in MF, so higher pressures are needed. UF is a process where the high molecular weight complexes (HMWC), such as protein, macromolecules, and suspended solids are rejected, while all low molecular weight complexes (LMWC) pass

through the membrane easily. There is consequently no rejection of mono- and di-saccharides, salts, amino acids, organics, inorganic acids or sodium hydroxide (Belfort et al., 1994). A typical application for UF is to remove large dissolved molecules that constitute the largest molecules of natural organic material (NOM).

In NF, the pore sizes are smaller than in UF, typically around 1 nm, which corresponds to dissolved compounds with a molecular weight of about 300. This makes NF suitable for the removal of relatively small organics, e.g., organic micropollutants and color from surface water or groundwater, and degradation products from the effluent of biologically-treated wastewater. Furthermore, NF membranes also have a surface charge, which remains in the presence of a feed solution. Therefore, the NF membranes do not work according to the principle of a sieving mechanism. The surface charge allows the removal of ions with a size below the pore size of the membrane. NF membranes can remove multi-valent (e.g., Ca^{2+} and SO_4^{2-}) ions.

RO membranes are dense membranes without predefined pores. As a result, permeation is slower and rejection is not a result of sieving, but of a solution-diffusion mechanism. RO membranes can remove most solutes including mono-valent ions (e.g., Na^+ and Cl^-). RO is the densest membrane, and only water can pass through it. The low permeability of RO membranes requires high pressures and, consequently, high-energy

consumption.

In summary, membrane filtration is a term used to describe the removal of particulates from feed water. MF and UF are the two processes that are most often associated with the term “membrane filtration.” UF and MF membranes remove diverse organic materials (which cause water color and odor problems), particulate materials (such as nano-sized and colloidal particles), and microorganisms (e.g., viruses, pathogens, bacteria, Giardia, and Cryptosporidium, so called biocolloids) via a sieving mechanism based on the size of the membrane pores relative to that of the particulate matter. For drinking water production, a MF or UF process is often used as pretreatment of a RO or NF process (the membranes typically last two or three years with proper operational conditions); without pretreatment, the RO or NF membranes are fouled in a short time and need to be replaced. NF and RO membranes can be used to desalinate seawater or brackish water.

2.2 Concentration Polarization and Membrane Fouling

Concentration polarization is the reversible build-up of dissolved or suspended solute. This build-up is due to the balance between the convective drag force toward the membrane surface and the back diffusion of particles from the region near the membrane

surface to the bulk phase. The presence of concentration polarization manifests in reduced permeate flux and hence the decrease of effective transmembrane pressure. If keep Continually increasing the applied pressure or increasing the permeate flux results in the membrane fouling.

Membrane fouling is defined as the build-up of materials on the membrane surface, such as adsorbed macromolecules, gels or deposited particles, and so on (Khulbe et al., 2000). There are several ways in which a membrane can become fouled. These include deposition of colloid particulates; precipitation of organic or inorganic materials; accumulation and attachment of biological growth; physical or chemical reaction of some feedwater components with the membrane surface itself; flocculation of organic or inorganic constituents to form large, insoluble polymers that will deposit on the membrane.

Fouling mechanisms include biofouling, organic fouling, inorganic fouling and particulate fouling. Membrane fouling may take the following forms:

- **Adsorption:** Adsorption occurs when attractive interaction between the membrane and the solute or particles exists. A mono-layer of particles and solutes can grow even in the absence of permeation flux leading to an additional hydraulic resistance.

If the degree of adsorption is concentration dependent, then concentration polarization exacerbates the amount of adsorption.

- **Pore blockage:** When filtering, pore blockage can occur leading to a reduction in flux due to the partial closure of pores.
- **Deposit:** Deposited particles can grow layer by layer at the membrane surface leading to an additional hydraulic resistance, which is often referred to as a cake resistance.
- **Gel:** The level of concentration polarization may lead to gel formation for certain macromolecules.

In MF and UF, cake growth is the main reason for membrane fouling. Different sizes of particles will form different configurations of cake layer. For monodisperse suspensions, small particles ($5-10nm$), which form cakes with high specific resistance, demonstrate a relatively fast approach to steady state. On the other hand, the time required to reach a steady state is the longest for particles favoring accumulation ($0.1-0.5\mu m$).

In crossflow MF, a fairly wide range of colloids and particles, such as colloids and bacteria, can lead to rapid membrane fouling. Early representative research works on MF membrane fouling include Milisic and Ben Aim (Milisic and Ben, 1986). They tried to

identify the particles and bacteria leading to rapid membrane fouling. Fane and Fell (Fane and Fell, 1987) focused on proteins leading to UF membrane fouling. In recent years, some researchers focused on the behavior of particle deposition on the MF membrane surface via direct observation through the membrane (DOTM) technique (Li et al., 1998). Vilker et al. (Vilker et al., 1981) studied UF membrane fouling via the optical shadowgraph technique. Baker et al. (Baker et al., 1995) studied the phenomena of NF membrane fouling. They studied the characteristics in NF used to treat surface water. In recent years, RO has become more popular for water reclamation and pollution control. Many researchers have dedicated themselves to studying the RO membrane fouling phenomena, transport mechanisms, and developing of membrane fouling models (Baker and Carnahan, 1991; Chen et al., 2004).

Several practical approaches can be pursued to reduce membrane fouling, among which modifying the chemical characteristic of the membrane surface is a very popular topic. The mechanism reduces the attractive forces or increases the repulsive forces between the solute and the membrane surface (Kim et al., 1988; Nystrom and Jarvinen, 1991; Kramer et al., 1989).

Although the effort of modifying the chemistry of the membrane surface is important to the application of membrane, it is not an effective and ultimate approach to

the membrane fouling problem. Effective cleaning methods are crucial for maintaining adequate long-term operation of all pressure-driven membrane processes. For practical applications, membrane backwashing is commonly used to recover the permeate flux. Backwashing during the membrane filtration process has been found to successfully remove most of the reversible components of the foulant layer (Smith, 2005). Backwashing also enables the system to operate for longer periods before intensive physical and/or chemical cleaning of the membrane is needed. However, determination of the interval between two successive backwashes is the key factor to backwash design. If the interval is too long, the cake layer on the membrane compacts and becomes increasingly difficult to remove during the backwash cycle. However, if the backwash is too frequent, it is a waste of energy and will hamper the efficiency of filtration, i.e., decreasing the amount of clean water product in a given period. Smith et al. (Smith et al., 2006) developed an approach to optimize the backwash, which is considered to be the most efficient technique for fouling minimization.

Although backwash is successful in removing the reversible component of the foulant layer, it demands higher energy and will affect the amount of clean water product, since down time is inevitable to completely stop the filtration processes and clean the membranes using backwashing. Therefore, many researchers investigated the optimum

operation condition to minimize the fouling by controlling the permeation rate.

2.3 Permeate Flux

Permeate flux, the rate of volumetric flow per unit membrane surface, is an important performance parameter in the design, operation, and evaluation of membrane filtration processes. The Darcy equation is the most general equation in the literature used to determine permeate flux, which is defined as

$$J = \frac{1}{A} \frac{\Delta P}{\mu(R_m + R_c)} \quad (2.1)$$

where ΔP is the transmembrane pressure (TMP), μ is the fluid viscosity, R_m the membrane resistance and R_c the cake layer resistance, which is further defined (Kim and Yuan, 2005) as

$$R_c = r_c \delta_c \quad (2.2)$$

$$r_c = \frac{9\phi_c}{2a^2} H(\phi) \quad (2.3)$$

where r_c is the specific cake resistance, δ_c is the cake layer thickness, a is the particle radius, and Ω is the Happel's Correction factor defined as (Happel, 1958)

$$H(\phi) = \frac{1 + \frac{2}{3}\phi_c^{3/3}}{1 - \frac{3}{2}\phi_c^{1/3} + \frac{3}{2}\phi_c^{5/3} - \phi_c^2} \quad (2.4)$$

Happel's Correction factor makes an adjustments to obtain the true hydrodynamic force experienced by particles within a porous medium (i.e., cake layer) of monodisperse suspensions.

Quantitative estimation of permeate flux requires consideration of different mass-transport mechanisms involved because the formation of a cake layer on the membrane surface and concentration polarization boundary layer near the membrane surface depend on back diffusion phenomena during the filtration process. Various theories of particle transport in low-pressure crossflow membrane filtration have been proposed over the previous three decades to describe permeate flux in crossflow filtration. The major differences in these models are the mechanisms of particle depolarization from the membrane region to the bulk flow. Mechanisms of particle transport and fouling in membrane filtration include: Brownian diffusion (Blatt et al., 1970; Porter, 1972), shear-induced diffusion (Zydney and Colton, 1986; Davis and Leighton, 1987; Davis and Sherwood, 1990; Romero and Davis, 1990), surface transport (Stamatakis and Tien, 1993), inertial lift (Green and Belfort, 1980), and concentrated flowing layers (Leonard and Vasilieff, 1984). Some reviews on the subject can be found elsewhere (Belfort et al., 1994; Bowen and Jenner, 1995; Wiesner and Chellam, 1999; Ripperger and Altmann, 2002). Sethi and Wiesner (Sethi and Wiesner, 1997) gave a copious review on the

literature of these transport mechanisms.

The back transport mechanisms of small molecular substances, macromolecules and colloids are different. Large particles are preferentially back-transported by shear-induced diffusion, whereas the transportation of materials with small sizes is mainly attributed to Brownian diffusion.

- ***Brownian diffusion***

The Brownian diffusion coefficient for spherical particle can be expressed by the Stokes-Einstein equation:

$$D_B = \frac{k_b T}{6\pi\mu_0\alpha_p} \quad (2.5)$$

where α_p is the particle radius, k_b is Boltzmann's constant, T is the absolute temperature, and μ_0 is the dynamic viscosity. Brownian diffusivity is inversely proportional to particle size, hence the smaller the particle is, the higher the diffusivity. Therefore, Brownian diffusivity is important for the solution of sub-micron particles.

- ***Shear-induced diffusion***

Shear-induced diffusion arises due to the random interactions between particles. These collisions between particles induce random movements of the particles within the

streamlines. Eckstein et al. (Eckstein et al., 1977) observed that a test particle in a suspension of rigid spheres migrated across the bulk streamlines in a uniform shear field produced by a Couette device. They measured the degree of migration and proposed an empirical correlation for the diffusion coefficient, D , as a function of shear rate, particle size, and suspension concentration:

$$D = 0.03\dot{\gamma}a_p^2 \quad (2.6)$$

where $\dot{\gamma}$ is the shear rate and a_p is the particle radius.

Ten years later, Leighton and Acrivos (Leighton and Acrivos, 1987) modified the expression by considering the particle concentration factor

$$D = \hat{D}(\phi)\dot{\gamma}a_p^2 \quad (2.7)$$

where ϕ is the particle volume fraction and $\hat{D}(\phi)$ is the dimensionless diffusivity, which can be expressed as

$$\hat{D}(\phi) = \frac{1}{3}\phi^2 [1 + 0.5\exp(8.8\phi)] \quad (2.8)$$

Therefore, when shear rate is increased, the particle back diffusion is enhanced accordingly. The degree of membrane fouling decreases, hence, the permeate flux increases.

Membrane fouling is related to the mechanisms of mass transport. When the back diffusion of particles increases, the degree of membrane fouling decreases. In crossflow

membrane filtration, particle deposition onto the membrane surface results from the drag force of the permeate flux. Therefore, permeate flux can be used as a design parameter to control membrane fouling. When the filtration is operated below a certain value of permeate flux, denoted as critical flux, membrane fouling can become negligible.

2.4 Critical Flux

According to an instructive review by Bacchin et al. (Bacchin et al., 2006), 10-20 papers related to the concept of critical flux were produced per year in recent years, and research in this area is still expanding. Presently, this concept is one of the most important dealing with fouling, which is not only demonstrated by the number of research papers produced per year, but also determined by the significance of the concept of critical flux itself. Critical flux is commonly coupled to the operation time to evaluate the actual flux “sustainability”.

Critical flux is defined in two ways. One way is to define it as the flux at which the transmembrane pressure starts to deviate from the pure water line, and/or the first flux for which irreversible fouling appears on the membrane surface. This is also called the strong form of critical flux. The other one is called the weak form, which assumes rapid initial fouling, bringing forth the relationship of flux versus transmembrane pressure

which will be located below the pure water line with a different slope. In general, critical flux can be defined as the “first” permeate flux at which fouling becomes noticeable. Practically, it can be defined as the borderline between non-deposition conditions and fouling conditions.

Early in the 1980s, some researchers suggested that low permeate flux can be used to control membrane fouling. This idea is the critical flux defined by Bacchin et al. (Bacchin et al., 1995). For a given suspension, the critical flux should be equal to the corresponding clean water flux at the same transmembrane pressure since it is defined as the permeate flux when fouling is negligible (Wu, 1999). Several methods can be used to determine the permeate flux value: direct observation through the membrane (DOTM), mass balance, flux-pressure observation, and so on.

2.4.1 Direct Observation through the Membrane (DOTM)

In DOTM, a microscope is used to observe the phenomena of particle deposition onto the membrane surface. Li et al. (Li et al., 1998) use a MF membrane, which is transparent when wet, in a crossflow test cell designed to allow optical observation through the membrane. They demonstrated that DOTM is a powerful technique for the study of particle deposition and interactions between the particles and the membrane

surface. Li et al. determined the critical flux of MF processes. The particles used in their experiments included yeast (mean diameter $5 \mu m$) and latex beads (3, 6.4 and $12 \mu m$). Li et al. (Li et al., 2000) applied the same technique to monitor the super-micron particles ($3-12 \mu m$) on MF membranes to identify the critical flux as a function of crossflow. Zhang et al. (Zhang et al., 2006) used this method to determine the critical flux of single-sized latex particles (3.0, 5.0 and $10.0 \mu m$) and mixed suspensions ($3.0+5.0$, $5.0+10.0$ and $3.0+10.0 \mu m$) during crossflow MF. Notably, the critical flux of single-sized particles was consistent with past studies in the literature. Therefore, the observation value of critical flux is instructive in optimizing the membrane filtration system.

2.4.2 Mass Balance

In this method, the passive adsorption of particles at no flux was measured and then any additional reduction of particles in the effluent was attributed to the deposition onto the membrane surface. In the research work of Kwon et al. (Kwon et al., 2000), a graph of flux against deposition rate was plotted after the deposition rate was determined using several fluxes. The critical flux was found by extrapolation. Gesan-Guiziou et al. (Gesau-Guiziou et al., 2002) found the critical flux of latex particles by combining the

mass balance and transmembrane pressure stepping method. In the work of Bowen et al. (Bowen et al., 2002), the same technique was used, i.e., they also plotted the deposition rate vs. the flux, then the extrapolation method was used to determine their critical flux.

2.4.3 Flux-Pressure Observation

In practical application, the critical flux value can be obtained from flux or pressure stepping tests. In these experiments, the critical flux can be determined either by imposing a pressure and measuring the flux, or measuring the pressure by imposing a flux. For both modes, the critical flux is the point where the flux-TMP relationship becomes non-linear. For the constant pressure method, the key point is to make sure the initial flux is lower than the critical flux. According to the research work of Miclent et al. (Miclent et al., 2001), critical flux is a function of crossflow velocity. When the velocity is 3 m/sec , critical flux is $20\text{ l/m}^2\text{h}$ ($5.5\ \mu\text{m/sec}$); when the velocity is 4 m/sec , critical flux is $50\text{ l/m}^2\text{h}$ ($13.8\ \mu\text{m/sec}$).

The flux stepping experiment is commonly used to determine the critical flux (Kwon et al., 2000; Manttari and Nystrom, 2000). There are two types experiments for flux stepping technique. One is to set the flux steps as a series of increasing flux step. The other one is to set the flux steps as a series of up-and-down flux steps. Stepping flux

method and stepping TMP method have different advantages and disadvantages, which can be seen in the description of next section, since the basic difference of these two methods lie in the constant TMP and constant flux operation modes.

Indeed, all of the methods of measuring critical flux only detect that the fouling rate is below a threshold of sensitivity for the method and the time scale used. This point needs to be kept in mind especially for those applications (e.g. water treatment) where the operating period between membrane cleaning can be long and/or a sudden change is suspected.

2.5 Constant TMP and Constant Flux Modes

Crossflow membrane filtration can be performed under conditions of either constant transmembrane pressure (TMP) or constant flux, which can be seen from Darcy's law. When TMP is constant, the membrane filtration is called constant TMP mode. In this mode, TMP is maintained constant throughout the filtration process. Therefore, the permeate flux decreases with time due to increased cake resistance. The TMP should remain constant with time, as any increase indicates fouling and therefore that the critical flux has been exceeded. Ideally, the total resistance should be calculated at each step to check whether the resistance has remained constant.

On the other hand, when permeate flux is constant, permeate flux is maintained constant throughout the filtration process. Increased applied pressure is required with time in order to maintain a constant permeate flux. Constant flux operation (with measurement of TMP) is readily achieved by pumping the permeate. These two modes have advantages and disadvantages.

For the conventional constant TMP mode of operation, the limitation is the changing conditions due to changing flux with time. However, constant TMP allows determination of a steady state flux (the filtration system is self regulated, as fouling decreases the flux thus reducing the rate of fouling), which leads to reliable results with no time dependence (if a sufficient duration for each pressure step is used). With this method, the steady state flux and then the steady state hydraulic resistance can be easily determined using Darcy's equation.

For constant flux experiments, with the presence of fouling phenomenon, a continuously increasing pressure with running time is requisite because of a (quasi) constant fouling rate. This method is able to determine the fouling rate, which is defined as the variation of the resistance with time for a fixed flux experiment. The dynamic data from the constant flux experiment allows one to have an idea about the sustainability of the process. This mode offers better control over the flow since the flow towards the

membrane is constant throughout the run. Another important aspect of constant flux operation is related to the concept of critical flux (Field, 1995; Wu, 1995; Howell, 1995), as described in the previous section of critical flux. Therefore, it is possible to obtain operation systems without fouling.

In general, constant pressure experiments can be recommended when working with suspensions containing components that show little tendency to adsorb onto the membrane, because steady state permeate fluxes will be achieved. On the other hand, it is easier for constant flux experiments to reveal fouling phenomenon as steady state fluxes may not be achievable. A flux may appear to be steady over a short time scale, but in reality, it may take a few days or weeks for the system to reach a steady state.

Gesan-Guiziou et al. (Gesan-Guiziou et al., 2002) used constant pressure experiments to determine the critical flux. An indication of fouling is then given by flux decline. So with certain feeds, permeate pumping is not essential, but for very sensitive determinations of critical flux constant flux operation is recommended because the sensitivity of the TMP measurement allows small changes due to any trace fouling to be detected.

2.6 Membrane Filtration Simulation

Numerical model is a fast and cost-effective way to gain a holistic understanding about membrane filtration processes. A traditional model or mathematical model, founded upon the generic principle, is commonly used to investigate the membrane filtration mechanism. This type of model focuses on the macroscopic phenomena of membrane filtration by integral methods. In general, parameters characterizing the physical processes are input into the governing equation. Kleinstreuer and Belfort (Kleinstreuer and Belfort, 1984) gave a good summary about the governing equations used in the membrane filtration. Then the governing equation is integrated by making many simplifying assumptions to produce a practical model used for design or prediction of performance.

2.6.1 *Conventional Mathematical Model*

Many authors focused on this research field, including the modeling of fluid flow in the membrane channel, mass transport mechanisms models, models used for predicting the permeate flux decline, concentration polarization models, cake layer formation models, models used for the measurement of critical flux, models for simulating membrane fouling mechanisms, and so on. Researchers developed mathematical models

for almost all these areas.

The fluid flow model is an important key in the development of membrane filtration processes because fluid flow provides the ambient environment for the whole system. Early in the 1950's, Berman (Berman, 1953) and Yuan and Finkelstein (Yuan and Finkelstein, 1956) used the perturbation theory to analyze 2-D flow in porous mediums. In order to make the problem tractable, some approximation assumptions are necessary, such as steady-state operation, incompressible fluid, laminar flow, fully developed parabolic flow, and uniform permeation flux along the flow channel. Most of these assumptions are too restrictive for practical applications. Therefore, many attempts have been made in order to reduce the number of assumptions. Belfort (Belfort, 1986) gave a detailed summary about these efforts. In 1994, Belfort (Belfort, 1994) provided a good review on this topic.

Mass transport is the basis for any permeate flux prediction model and fouling mechanism model. Concentration polarization model or film theory can be used to predict the steady state MF flux. At steady state, the convection of particles toward the membrane is balanced by diffusion away from the membrane and their convection toward the channel exit by crossflow. Porter (Porter, 1972) integrated the one-dimensional convection-diffusion equation across the polarization boundary:

$$J = k_f \ln \left(\frac{\phi_w}{\phi_b} \right) \quad (2.9)$$

where J is the permeate flux, ϕ_w and ϕ_b are the particle volume fractions at the edge of the cake layer and in the bulk suspension, respectively, k_f is a mass transfer coefficient dependent on the membrane channel dimension, particle diffusivity, and shear rate. For solutions with smaller particles, e.g. sub-micron particles, Brownian diffusivity is dominant. Later, researchers modified this mathematical model by including the diffusion coefficient. But the prediction was not complete until the shear-induced diffusion, inertial lift, and surface transport were introduced to modify the conventional numerical model.

Mathematical models focused on predicting permeate flux decline include the work by Kozinski and Lightfoolt (Kozinski and Lightfoolt, 1972). They developed a theoretical model for predicting permeate flux using a rotating disk UF membrane that included concentration dependent diffusivity and viscosity. Later, as more and more formulated models were developed, all of these models contributed to a better understanding about membrane filtration. In 1982, Hermia (Hermia, 1982) developed a model used to predict permeate flux decline, which is one of the models obtained from conventional filtration theory. In 1995, Bowen and Jenner (Bowen and Jenner, 1995) wrote a good review paper,

which presented an assessment of the existing filtration models for colloidal and fine particle dispersions with emphasis on their qualitative and quantitative predictive capability, scientific basis, and limitations. The model developed by Duclos-Orsello et al. (Duclos-Orsello et al., 2006) included all three classic membrane fouling mechanisms, (pore blockage, pore constriction, and cake formation), to describe flux decline behavior during the MF process. Kanani and Ghosh (Kanani and Ghosh, 2007) developed a model used for predicting the permeate flux decline for constant pressure UF, which considered the interplay between permeate flux, concentration polarization, and membrane fouling.

Since 1995, when critical flux was first defined by Field and Wu (Field and Wu, 1995) and Howell (Howell, 1995), more and more researchers have turned their attention to modeling of critical flux. In 2002, Ho and Zydney (Ho and Zydney, 2002) developed a mathematical model to describe the change in TMP during constant flux MF. Their simulations provided important insights into the design and operation of constant flux MF processes. However, according to the definition of critical flux, the forces pushing the particles towards the membrane exactly balance the back transport forces that push the particles away from the membrane. Without considering the electrostatic interactions, the back transport mechanism could be inertial lift or shear-induced diffusion depending on the particle size. Therefore, most of the research work on the critical flux model is based

on the advances in mass transport mechanism.

In the last three decades, numerous advances have been achieved in the modeling of membrane filtration mechanisms. Mathematical models together with experiments are the foundation of the development of membrane filtration processes. However, fouling mechanisms, parameters that may lead to the decline of permeate flux, and the interrelation among these parameters are still areas with high expectations and insufficient results. Due to the need for a large number of computations, many approximations must be made in order to get a numerical solution to the governing equations. Compared to these theoretical mathematical models, Computational Fluid Dynamics (CFD) yields a more precise solution to help understand these complex processes by reducing the number of approximations.

Computational Fluid Dynamics (CFD), a software model, is an important tool used for developing the movement of particles in a membrane filtration system. It allows the modeling of many situations provided suitable computing power is available. The computations for the movement of the particle in a membrane filtration system will take into account the flow, the bulk region of the membrane channel, boundary layer, transport mechanisms, and the electrostatic, chemical and physical interactions at the membrane surface. All of these processes are interdependent and non-linear. CFD combines these

processes to perform numerical simulations.

Many authors (Fimbres-Weihs and Wiley, 2007; Ghidossi et al., 2006; Ranade and Kumar, 2006; Rahimi et al., 2005) used CFD software packages to investigate the mass transport within the membrane channel to predict the permeate flux. Other authors (Santos et al., 2007) are interested in the simulation of flow conditions, and they used CFD to calculate the flow and concentration fields in side membrane module channels. Their computational results gave excellent agreement with experimental results. Bacchin et al. (Bacchin et al., 2006) developed a numerical simulation using CFD modeling to investigate the critical flux for colloidal dispersion filtration. Schwinge et al. (Schwinge et al., 2002) used CFD to investigate the effect of spacer filaments on flow patterns in narrow channels. In this research, both sub- and supercritical flow patterns were examined.

CFD provides more precise solutions to the governing equations of membrane filtration processes compared to theoretical mathematic models. However, CFD is based on small computational demands. It cannot combine all of the possible mass transport mechanisms and interaction forces among particles into a model. In 1990, Romero and Davis (Romero and Davis, 1990) developed a transient model for crossflow for MF based on a shear-induced hydrodynamic diffusion mechanism of particle motion within a

concentrated flowing layer near the membrane surface. Later, Sethi and Wiesner (Sethi and Wiesner, 1997) produced a unified transient model based on the formulation developed by Romero and Davis by including the effects of Brownian diffusion, inertial lift, and shear-induced diffusion.

Although conventional mathematical models, CFD models, and unified computer models have provided important insights into particle motion in crossflow membrane filtration, they can only examine the macroscopic phenomena in a filtration system. In order to obtain a more fundamental understanding of particle behavior in crossflow, such as phenomena of fouling material trajectory and phenomena of particulate material deposition onto the membrane surface, precise microscopic-scale models are greatly necessary.

2.6.2 *Monte Carlo Simulation*

Brownian Dynamics (BD), Molecular Dynamics (MD), and Monte Carlo algorithms have proven to be exceptional analytical tools for probing discrete molecular, ionic, and colloidal motions at basic microscopic levels. They offer the advantages of studying discrete particle trajectories, inter-collision among particles, and configurations of particle systems on a precise microscopic scale. These models subdivide the whole

macroscopic system into individual underlying constituents that contribute the whole system. Therefore, system performance can be understood and interpreted with great precision and exactness. BD demonstrates advantages over MD by its capacity for time-scale separation. MC exhibits strengths in terms of ease of implementation. Chen and Kim (Chen and Kim, 2004) gave an copious review on the modeling methods of BD, MD, and MC.

Tung et al. (Tung et al., 2006) used MD and MC simulations to investigate the effect of solvent types on the morphology of free volume as well as the gas transport properties in polymethylmethacrylate (PMMA) membranes from a microscopic viewpoint. The effects of solvent types on the sorption of oxygen molecules in a-PMMA membranes were conducted using the MC simulation method. MD and MC simulations were carried out by Takaba et al. (Takaba et al., 2006) to investigate the effect of intercrystalline region structure on the diffusivity and adsorption parameters for methane in silicalite.

Since MC has the advantage of easy implementation, it is widely used to investigate the membrane fouling phenomena in the membrane filtration process for water and wastewater treatment. Flora (Flora, 1993) developed a stochastic model using MC methods to investigate the flux decline caused by surface fouling of pores in UF membranes from a microscopic viewpoint. And this model was verified by experiments

implemented in a dead-end batch assembly. In the work of Kim and Hoek (Kim and Hoek, 2002), MC simulations were performed to predict volume fractions and corresponding radial distribution functions which represent the effect of particle size, ionic strength, zeta potential, and applied pressure on the cake structure. Then the influence of all of these factors on permeate flux decline was qualitatively predicted. Compared to previous experiments, the simulation method provided very good prediction of cake porosity as well as the permeate flux under the dead-end operation condition.

Chen and Kim (Chen and Kim, 2006) planned to achieve a total mirror reflective MC model to simulate the real situation occurring in a long crossflow open channel filtration system. The real situation included continuous fully developed 3-D parabolic flow field, dilute bulk solution, spatial variations in cake layer thickness, resistance, and permeate flux. However, it is an enormous project to develop such a comprehensive model. They separated the development process into several stages.

After a comprehensive literature review on the theories and algorithms for three microscopic modeling techniques, i.e., BD, MD, and MC simulation. Chen et al. (Chen et al., 2005) developed a MC model and applied this model to investigate the phase transition from a fluid-like polarization layer to a solid cake layer of particle deposits during dead-end membrane filtration system of interacting colloidal particles. In this

model, an MC algorithm was modified into a biased MC method (Kim et al., 2001). The model was effective in demonstrating the roles of the hydrodynamic drag force and inter-particle potential in governing the volume fraction of particle deposition. Hence, it demonstrated that the problem of colloidal membrane filtration casts hydrodynamic bias MC simulation is an extremely advantageous alternative that possesses the efficacy to capture the minute details of every distinct force and particle displacement in colloidal membrane filtration.

The objective of the third stage (Chen et al., 2006) was to bring the model into a long open channel crossflow membrane filtration unit. However, the simulation was still focused on a small section of the long channel. Compared to the second stage, the additional features of the third stage include the fully developed parabolic flow field and spatially varying cake thickness. Thus, the model became more comprehensive in the scope of physical processes. By using this model, they observed the mono-layer fouling phenomena. Even when the parameters were changed, obvious particle accumulation was still not observed. In order to mimic the cake formation, a periodic boundary condition was applied, i.e., taking the particles that have exited the outlet and re-circulating them back upstream where they re-enter the membrane channel.

According to the plan of the model development, the last stage is to develop a

comprehensive model to mimic the real situation occurring in the crossflow membrane channel. When the real boundary condition was applied to the model, i.e., adding a feed tank upstream to feed the membrane channel, no matter how to change the input parameters were changed, cake formation or the serious membrane fouling phenomena was still not observed. Therefore, due to the problem that particles in an open membrane channel system will readily exit without accumulating on the membrane surface, further investigation with respect to the particle transport mechanism in a crossflow open channel is still necessary.

The objective of this study is to develop a large scale Monte Carlo simulation for crossflow membrane filtration. In this model, Brownian and shear-induced diffusion are incorporated into an effective hydrodynamic force exerted on the hard spheres in a concentrated shear flow. The effects of shear rate and particle size on the critical flux are carefully examined. This model is used to identify the critical flux in terms of the particle size and shear rate by looking into the dynamic particle structures associated with the critical flux. Then the estimated critical flux is compared to that obtained from experimental observations.

CHAPTER 3. SIMULATION METHOD

3.1 Ambient Flow Field

The membrane filtration system is an open one in this study. Basically, the particle movements are biased in the direction of the flow field. Figure 3.1 shows the streamlines in the membrane channel, which were calculated by Berman (1953) using perturbation theory and can be readily applied to crossflow membrane filtration. The velocity along the x - and y - directions is shown as:

$$u(x, \eta) = \bar{u} \left(1 - \frac{v_w x}{uh} \right) \left[\frac{3}{2} (1 - \eta^2) \right] \left[1 - \frac{\text{Re}}{420} (2 - 7\eta^2 - 7\eta^7) \right] \quad (3.1a)$$

$$v(\eta) = v_w \left[\frac{\eta}{2} (3 - \eta^2) - \frac{\text{Re}}{280} \eta (2 - 3\eta^2 + \eta^6) \right] \quad (3.1b)$$

with

$$\eta = \frac{z}{h} \quad (3.2)$$

where \bar{u} is the average crossflow velocity, v_w is the permeate velocity of an order of $O(10^{-5} - 10^{-6})$ m/sec, $h(=H/2)$ is the half-height of the channel of an order of $O(10^{-2} - 10^{-3})$ m, and Re is the permeate Reynolds number defined as:

$$\text{Re} = \frac{v_w h}{\nu} \quad (3.3)$$

where ν is the kinematic viscosity. By taking the typical values of $v_w = O(10^{-5} - 10^{-6}) \text{ m/sec}$, $h = O(10^{-2} - 10^{-3}) \text{ m}$, and $\nu \approx 10^{-6} \text{ m}^2/\text{sec}$, we neglect terms containing Re in equation (3.1) for u and v , and then assume

$$\frac{v_w l}{u h} \ll 1 \quad (3.4)$$

where l is the membrane length. Then the flow velocity is approximated as:

$$u(\eta) = \bar{u} \left[\frac{3}{2} (1 - \eta^2) \right] \quad (3.5)$$

$$v(\eta) = v_w \left[\frac{\eta}{2} (3 - \eta^2) \right] \quad (3.6)$$

3.2 Modeling System

An intermediate section of the entire crossflow membrane channel is selected to investigate the critical flux of hard sphere suspension. This section of the membrane channel is denoted as simulation box as shown in Figure 3.2. In this simulation, only the hard sphere suspension case is considered, so each particle experiences three forces in the direction normal to the membrane surfaces: hydrodynamic drag force F_d , gravitational force F_g , and buoyant force F_b . Therefore, the total force acting on each particle F is the summation of these three forces.

$$\mathbf{F} = \mathbf{F}_g + \mathbf{F}_b + \mathbf{F}_h \quad (3.7)$$

$$\mathbf{F}_g = -\frac{4\pi}{3}a^3\rho_p g \hat{z} \quad (3.8)$$

$$\mathbf{F}_b = +\frac{4\pi}{3}a^3\rho_f g \hat{z} \quad (3.9)$$

$$\mathbf{F}_h = \frac{k_b T v(\eta) K^{-1}(\phi)}{D_B + D_{st}} \hat{z} \quad (3.10)$$

where a is particle radius, η is the dimensionless distance from the membrane surface, v is the velocity along y-direction, ρ_p and ρ_f are mass densities of the particle and fluid, respectively, g is the gravitational acceleration, k_b is the Boltzman constant, T is the absolute temperature, $K(\phi)$ is sedimentation coefficient, and D_B and D_{st} are the Brownian and shear-induced diffusivities, respectively. D_B and D_{st} can be represented as:

$$D_B = \frac{k_b T}{6\pi\mu a} S(\phi) \quad (3.11)$$

$$D_{st} = \dot{\gamma}(\eta) a^2 \hat{D}(\phi) \quad (3.12)$$

where

$$S(\phi) = \frac{\partial \phi Z(\phi)}{\partial \phi} \quad (3.13)$$

and $Z(\phi)$ is the osmotic compressibility (Hansen and McDonald, 1976). However,

$S(\phi)$ is omitted in this simulation, i.e.,

$$D_B \rightarrow \frac{k_b T}{6\pi\mu a} \quad (3.14)$$

For $\hat{D}(\phi)$, because the random trial movement implicitly includes the entropic contribution stemming from the particle configuration gradient, among various results from experiment and simulation studies, the most widely accepted one (Leighton and Acrivos, 1986; Leighton and Acrivos, 1987; Leighton and Acrivos, 1987) is used in this simulation:

$$\hat{D}(\phi) = \frac{1}{3}\phi^2 \left(1 + \frac{1}{2}e^{8.8\phi} \right) \quad (3.15)$$

Heppel's sphere-in-cell model (Happel, 1958) is incorporated in this study to estimate the sedimentation coefficient, which decreases with the increase of volume fraction ϕ :

$$K^{-1}(\phi) = H(\phi) = \frac{6 + 4\phi^{5/3}}{6 - 9\phi^{1/3} + 9\phi^{5/3} - 6\phi^2} \quad (3.16)$$

Detailed discussion on hydraulic force equation and its application to colloidal filtration can be found elsewhere (Kim and Liu, 2007; Sierou and Brady, 2004). $\dot{\gamma}$ is the shear rate at a dimensionless distance η from the membrane surface, which is calculated as:

$$\dot{\gamma}(\eta) = \frac{1}{h} \frac{du}{d\eta} = -\eta \frac{3\bar{u}}{h} \quad (3.17)$$

where \bar{u} is the average crossflow velocity. The shear rate reaches its maximum in magnitude on the membrane surfaces (when $\eta = \pm 1$) and vanishes near the membrane channel epicenter (when $\eta = 0$). The shear rate varies with the normal distance from the membrane surface.

3.3 Biased Probability Distribution

Biased probability distribution is considered in this simulation. There are two components for the biased probability distribution, transverse and longitudinal biases. Tangential bias results from the crossflow, while the vertical bias is caused by the permeate flux. The orders of magnitude are dissimilar between permeate flux and crossflow velocity. Therefore, these two components are separately implemented in MC simulations.

3.3.1 Tangential Bias

In the crossflow membrane channel, the movement of particle in x -direction is highly subject to ambient crossflow since the crossflow is much faster than permeate flux.

Therefore, particle transport due to Brownian diffusion is negligible near the epicenter of the membrane channel. The simulation allows for movement of particles only in the direction of the crossflow. Hence, the transport is convection-dominated, i.e., the movement occurs only in the positive x-direction. However, on the membrane surface, a no-slip boundary condition is used since the flow velocity is close to zero. It is easy for particles to perform their random Brownian motion. Therefore, the spatial probability distribution of a particle is 50 to 50 percent. Then the transport is influenced by diffusion.

Considering the dominant transport mechanism described above, the random displacement of each particle, i.e., the movement of particle from an old position r_{old} to a new position r_{new} , can be expressed as follows:

$$\Delta x = x_{new} - x_{old} = a_0 (2N_{rand} - 1 + P_x) \quad (3.18)$$

$$\Delta y = y_{new} - y_{old} = a_0 (2N_{rand} - 1) \quad (3.19)$$

$$\Delta z = z_{new} - z_{old} = a_0 (2N_{rand} - 1) \quad (3.20)$$

where a_0 is the maximum displacement of the random movement (adjusted during the simulation to maintain the acceptance ratio of the random transition close to 0.5), N_{rand} is the a random number generated using the intrinsic Fortran 90 function, **rand**, and P_x is the axial transition probability, which readily includes the crossflow influence on

particle movement:

$$P_x = \frac{u(\eta)}{u_{\eta=0}} = 1 - \eta^2 \quad (3.21)$$

Hence, near the epicenter of membrane channel, i.e., $\eta = 0$,

$$\Delta x = x_{new} - x_{old} = a_0 (2N_{rand}) \quad (3.22)$$

while, on the membrane surface, i.e., $\eta = 1$,

$$\Delta x = x_{new} - x_{old} = a_0 (2N_{rand} - 1) \quad (3.23)$$

The transport mechanism described above is shown in Figure 3.3. Near the epicenter of the membrane channel, particle movements are allowed only in the crossflow direction. Therefore, the probability of particle movement along the $+x$ and $-x$ directions is 1.0 and 0.0, respectively. On the membrane surface, it is easy for particles to perform Brownian motion, i.e., the particles can move in either the crossflow direction or the opposite direction of crossflow. And the probability along each direction is 50 to 50 percent. Between the epicenter and the membrane surface, diffusion and convection are equally important.

3.3.2 Normal Bias

Along the normal direction, each particle experiences gravitational force, buoyant force, and hydrodynamic drag force, which engender the normal transition probability.

The transition probability is determined to be:

$$P_z = \min[1, \exp(-\beta\Delta E - \beta\lambda F \cdot \Delta \mathbf{r})] \quad (3.24)$$

where $\beta = \frac{1}{k_b T}$, λ (=0.5) is the force bias parameter in Monte Carlo simulation, $\Delta \mathbf{r}$ is the random displacement,

$$\Delta \mathbf{r} = \mathbf{r}_{new} - \mathbf{r}_{old} \quad (3.25)$$

ΔE is the energy difference between the new and old particle positions. In this hard-sphere suspensions case, ΔE is set to zero unless overlap occurs among particles.

When the particle moves from an old position \mathbf{r}_{old} to a new position \mathbf{r}_{new} , a random number is generated. Then the transition probability P_z is compared with the random number. If the random number is less P_z , then the trial movement is accepted and the particle moves to the new position \mathbf{r}_{new} ; otherwise, the movement is rejected, and the particle still stays at the old position. If the particle overlaps with the other particles when it moves to a new position, the trial movement is immediately rejected because this situation is equivalent to that when the $\Delta E \rightarrow \infty$, which is thermodynamically forbidden.

3.4 Parallel Algorithm

3.4.1 Domain Decomposition

In this simulation, every individual replacement of a particle is computed discretely. Therefore, a large amount of computational power is demanded. A parallel computer is used to implement the computation. The whole membrane channel is divided into several domains, termed domain decomposition. Then each processor is responsible for the computations in one domain. The decomposition is only limited along the tangential direction (i.e. x -direction) since the particle distribution is non-uniform along vertical direction (i.e. z -direction) due to the deposition of the particle onto the membrane surface. Therefore, near the membrane surface, particle concentration is much higher compared to the bulk phase or in the middle of the membrane channel. If the membrane channel is decomposed along the vertical direction, after each iteration step of particle movement, the particle number must be checked, if necessary, and the domain has to be re-decomposed in order to maintain the load balance for each processor, which is time consuming. However, if the domain decomposition is only along the x -direction, load balance is not a concern for parallel programming since the particles are uniformly distributed along the horizontal direction. Figure 3.4 is the diagram of domain decomposition among four processors. Each domain is called a simulation cell. In this

model, the number of processors can be arbitrary according to the requirements of simulation scale.

3.4.2 *Communications Among Processors*

If the domain decomposition is only limited to the x – direction, the load is almost always in balance for each processor. However, each processor is not totally independent of the other processors because the particles near the boundary of the simulation cell may move to the neighboring processors. Even if the particle center still remains in the original simulation cell, overlap with particles in the neighboring cell could happen. So communication is necessary among neighboring simulation cells. The computational method employed to perform the simulations is parallel programming via Message Passing Interface (MPI).

A master-slave parallel algorithm is used in this model. Figure 3.5 shows the schematic diagram among the processors. One of the processors functions as the server (or master), while the remaining processors are referred to as workers or slaves. The master performs the task decomposition and output, providing the data for slave nodes. Slave nodes are responsible for the computation in each simulation cell. For each iteration step, once the slave nodes finish the computation, they send the data back to the

master. In the mean time, the master receives data and re-decomposes the task, then sends the data to slave nodes to start the next iteration step.

3.5 Initialization of Simulation

3.5.1 Dimension of Membrane Channel

The membrane channel is referred to as a simulation box in this study. The box dimension is $L \times W \times H$, where L , W , and H are the length, width, and height, respectively. Generally, H is set to 7 times the width. In this way, it is more convenient to monitor the particle transport phenomena along z - direction in the membrane channel, especially the concentration polarization, which is possibly followed by cake formation. The length of simulation box, i.e. L , is set to be at least 3 times longer than the width W . In this way, it is easy to monitor the particle transport phenomena along z -direction.

3.5.2 Initial Volume Fraction

Initial volume fraction ϕ_{in} is arbitrarily assigned between 0.01 and 0.1, which is higher than a typical feed volume fraction. Generally, the feed water has a volume fraction of an order of $O(10^{-3} - 10^{-5})$. In this way, Monte Carlo simulation is sped up, i.e., the filtration system can reach a dynamic equilibrium state in a relatively short time

without affecting the spatial configuration of particles. With an educated guess of the initial volume fraction, a dynamic equilibrium configuration will yield a dense solid-like structure on the membrane surface and a liquid-like solution near the channel center representing the feed suspension.

3.5.3 *Boundary Condition*

At the beginning of the simulation, randomly generated particles are populated without overlap in the simulation box. In order to mimic the spatial homogeneity, the periodic boundary condition is used along the x - and y -directions, which means when the particles exit from one side of membrane channel, they will be forced back into the channel from the other side. The periodic boundary condition in the x -direction implicitly assumes that the thickness of the concentration polarization layer or cake layer is locally constant along the crossflow direction, and the boundary condition in the y -direction (perpendicular to the crossflow direction) indicates the absence of any wall effects. The diagram is shown in Figure 3.2(b) shows the boundary condition along z -direction. If a particle escapes from the bottom or the top of the membrane surface, it will be bounced back into the membrane channel. The location in the $x-y$ plane is the same as the projected displacement of the old position.

CHAPTER 4. RESULTS AND DISCUSSION

4.1 Verification of Transport Mechanisms

In this simulation, a canonical ensemble is used in which the total number of particles, representative volume of system, and the temperature are constant. In this canonical simulation, the number of particles is fixed at 2100. The particles are hard-spheres. The initial volume fraction is 0.1, which is much higher than the typical feed volume fraction. In this way, particles are rapidly pushed toward the membrane surface by using the inverse sedimentation coefficient as shown in equation (3.16), which means that most particles deposit onto the membrane surface in a short duration time and only a small fraction of particles are left in the epicenter of the membrane channel. The purpose of the higher initial volume fraction is to render an acceptable concentration gradient along the direction normal to the membrane surface since a small volume fraction close to the feed volume fraction would not provide meaningful results. However, if the initial volume fraction is too high, severe deposition will occur through the sedimentation coefficient, i.e., the simulation may exaggerate the fouling phenomena.

Figure 4.1 shows the results of the canonical Monte Carlo simulations with various permeate flux values. When the permeate flux v_w is set to $0 \mu m / sec$, relatively homogeneous particle configuration as shown in Figure 4.1(a) is visually observed in the membrane channel. Permeate flux is set to $1 \mu m / sec$ (Figure 4.1(b)), where some particles moving towards the membrane surface can be observed. However, it is still relatively homogeneous distribution. As the permeate flux continually increases, i.e., when $v_w = 5 \mu m / sec$, deposit phenomena becomes more clear as shown in Figure 4.1(c). The configuration of two major groups of particles clustered near the double-membrane surfaces can be observed. Figure 4.1(d) and Figure 4.1(e) show the more realistic profiles of particle distribution along the direction normal to the membrane surface. When permeate flux is set to be $30 \mu m / sec$, almost all particles deposit onto the membrane surface, which is called bisection particle configuration as shown in Figure 4.1(f). Therefore, permeate flux with a value of $30 \mu m / sec$ causes significant fouling in terms of particle deposition or cake formation.

Under the double-membrane configuration, as the permeate flux increases, symmetric particle configuration is formed. Figure 4.2 shows the symmetric volume fraction profiles with different permeate fluxes when particle radius is $0.1 \mu m$ and the shear rate is $1000 / sec$. The particles are almost homogeneously distributed throughout

the simulation box when the permeate flux is absent. However, the concentration is higher near the membrane surfaces compared to the rest part of membrane channel, which can be attributed to the reflection effect of the boundary under fast crossflow operation conditions. The wall concentration is always greater than the bulk concentration even under the condition of minimal presence of permeate flux and without any adsorption mechanism.

The local volume fractions near the epicenter can be interpreted as the feed volume fraction as shown in Figure 4.2. For example, the cases of permeate flux of $10 \mu\text{m} / \text{sec}$ and $20 \mu\text{m} / \text{sec}$, which corresponds to Figure 4.1(d) and Figure 4.1(e), respectively, can be interpreted as the crossflow filtration with feed volume fraction (ϕ_{feed}) of 0.01 and 0.004, and cake volume fraction (ϕ_{cake}) of 0.34 and 0.40, respectively. Fluctuations of volume fraction near the epicenter, as observed in the cases when permeate flux is $20 \mu\text{m} / \text{sec}$ and $30 \mu\text{m} / \text{sec}$, originate in the sparse particle distribution in the center area.

This simulation is also used to investigate the effect of shear rate on the particle distribution pattern. When the shear rate is increased to $5000 / \text{sec}$ as shown in Figure 4.3, the profile pattern of particle distribution along the direction normal to the membrane surface is very similar to the case when the shear rate is $1000 / \text{sec}$ as shown in Figure

4.2. However, when the shear rate increases, more particles are diffused back to the bulk phase instead of depositing onto the membrane surfaces, hence, resulting in smaller values of volume fraction on the membrane surface. It can be seen that from Figure 4.2, permeate fluxes of 20 and 30 $\mu\text{m} / \text{sec}$ cause the cake volume fractions of 0.40 and 0.43, respectively. When the shear is increased as in Figure 4.3, the same permeate fluxes generate the cake volume fractions of 0.325 and 0.362, respectively. Therefore, it can be further confirmed that the effective force, which is derived as equation (3.10), well accurately represents the significance of shear-induced diffusion outweighing that of Brownian diffusion for micro-particles.

It can be concluded that the simulation is reasonable with respect to particle configuration for different permeate fluxes, the volume fraction profiles in the direction normal to the membrane surfaces with various fluxes, and the effect of shear rate on the cake volume fraction.

4.2 Order Parameter

In the last section, the spatial distribution of particles either uniform or in a bisected configuration is based on visual estimation. In thermodynamics, order parameter is often used as a rigorous tool to determine this kind of phase transition phenomena. The order

parameter is the quantity that is indeterminate at the critical point (the point of the phase transition), which is used to denote “a fluctuating variable of which average value provides a signature of the ordered state (or broken symmetry) in the system” (Barrat and Hansen, 2003). In the culture of crossflow membrane filtration, the critical point is often referred to the critical flux. Once an order parameter is chosen, it should have the capability of easy calculation and be able to extract meaningful physics information that would be used to determine the critical flux.

In this study, the variance of the particle distribution is proposed as the order parameter for crossflow filtration:

$$\psi = \frac{\langle (z - \hat{z}) \rangle}{h^2} = \frac{1}{N_p} \sum_{i=1}^{N_p} \left(\frac{z_i - \hat{z}}{h} \right)^2 \quad (4.1)$$

where z_i is the z -coordinate of the i^{th} particle, and \hat{z} is the mean z -coordinate of the N_p particles. For a homogeneous (aligned) distribution, i.e., when volume fraction is a constant, the value of ψ converges to $1/3$, proven as follows:

$$\psi \approx \frac{1}{N_p} \sum_{i=-N_p/2}^{N_p/2} \left(\frac{\delta z}{h} \right)^2 i^2 \approx \left(\frac{N_p \delta z}{2h} \right) \left(\frac{1}{3} \right) \approx \frac{1}{3} \quad (4.2)$$

where $z_i = i(\delta z)$, and δz is the normal distance between two nearest neighbors in the aligned configuration. For non-uniform distribution, when more particles are pushed downward to the membrane surfaces by the permeate flux, \bar{z} is close to zero due to the

vertically symmetric particle configuration as shown in Figure 4.1. The presence of particles near the membrane surfaces contributes to an increase of ψ from its minimum value of $1/3$. Therefore, the increase in ψ value indicates that more particles are being dragged away from the epicenter of the membrane channel. Therefore, the particle distribution deviates from the homogeneity of the initial configuration.

Figure 4.4 shows the order parameter defined as in equation (4.1) versus the permeate flux for different size particles ranging from 0.1 to $10.0 \mu m$. For each case, 12 permeate fluxes were chosen to calculate the order parameter. The permeate fluxes are $0.0 \mu m / sec$, $5 \mu m / sec$, $10 \mu m / sec$, $20 \mu m / sec$ and so on in $10 \mu m / sec$ increments up to $100 \mu m / sec$. Each point in Figure 4.4 is calculated from a simulation run using 2100 particles. The shear rate is $3333.3 / sec$.

As shown in Figure 4.4, the cases with smaller particles, ψ appears to rapidly increase when the permeate flux is less than $20 \mu m / sec$, then reaches a plateau when the permeate flux is close to $100 \mu m / sec$. This rapid increase in ψ at lower flux attenuates as the particle size increases from 0.3 to $10.0 \mu m$. It can be seen from this figure that ψ is greater than $1/3$ for all of the calculations, which indirectly confirms that the order parameters are appropriately calculated. As to the deviation of ψ from $1/3$ with zero permeate flux, it indicates that the wall concentration is higher than the bulk

concentration as discussed in the previous section. This phenomena is important only when the feed volume fraction is more than a few percent (volume to volume) because the particles lose their degrees of freedom in the presence of the membrane, which acts as a geometrical barrier.

It can also be noted from Figure 4.1 that the ψ value with particle size of $0.1 \mu m$ behaves different from the other four curves by intersecting with them, while the other four curves are clearly stratified in an organized manner with respect to particle size. This demonstrates that the dominant transport mechanism for particles $0.1 \mu m$ is different from the other four cases. It can be inferred from this that $0.3 \mu m$ particles can be a delineation between Brownian and shear-induced diffusion with the shear rate of 5000/sec. Different shear rates will change the magnitude and variation of ψ with respect to permeate flux.

It is assumed that the order parameter of ψ represents information about particle configuration characteristics so that it can be used to estimate the critical flux. Close examination of Figure 4.1 shows that there are two distinct regions in terms of variational behavior of ψ : regimes of acclivity and plateaus at low and high fluxes. However, the variation of ψ is too smooth to determine the point of permeate flux that can clearly discriminate two different phases of particle distributions, i.e., essence uniform and

conspicuously bisected. Therefore, ψ in Figure 4.4 is numerically differentiated with respect to permeate flux v_w , and the results are shown in Figure 4.5.

As expected, it can be seen from Figure 4.5 that $d\psi/dv_w$ is high for the low flux, or vice versa. A higher value of $d\psi/dv_w$ indicates the sensitive changes of ψ with respect to v_w , and negligible $d\psi/dv_w$ means a minute change in structures from that of $v_w = 0$. The offset of $d\psi/dv_w$ on the v_w -axis is not clear in Figure 4.5. Therefore, a linear regression is performed using the first three points of each curve. The dotted lines show the linear regression plots, and the x -intercept asymptotically delineates transition points of $d\psi/dv_w$ from finite to vanishing values. Therefore, each curve in Figure 4.5 can be divided into two regions, i.e., linear decline region and zero-slope region. Offset points can be interpreted as fluxes of phase transition, of which trend is analogous to the second order phase transition (Barrat and Hansen, 2003), in which the second order derivative of the order parameter is discontinuous near the transition point. The variation of $d\psi/dv_w$ can be simplified as:

$$\frac{d\psi}{dv_w} = \begin{cases} -C_1 v_w + C_2 & \text{for } v_w < J_{crit} \\ 0 & \text{for } v_w > J_{crit} \end{cases} \quad (4.3)$$

where C_1 and C_2 are constants to be determined by linear regression. J_{crit} is defined as the permeate flux when $d\psi/dv_w$ first becomes zero as the permeate flux (v_w)

increases from zero:

$$J_{crit} = C_1 / C_2 \quad (4.4)$$

It can be seen from equation (4.3) that the second order derivative of the (linearized) order parameter (ψ) gives a discontinuous point where the permeate flux (v_w) equals to the J_{crit} . Therefore, the method of determining critical point of second phase transition is used to approximately estimate the critical flux in this simulation.

4.3 Critical Flux

The critical flux J_{crit} , which is determined using the method described in the last section, is plotted with respect to particle size as shown in Figure 4.6. The determination of each critical flux value in this figure requires series simulations with a fixed value of particle diameter and varying permeate fluxes for the phase transition analysis using equation (4.3). Altogether, 60 simulation runs for five different particle diameters with twelve permeate fluxes were implemented to obtain the critical flux values shown in Figure 4.6. The estimated critical flux is compared to the experimental results of Kwon et al. (Kwon et al., 2000), which are also plotted in Figure 4.6.

Two definitions of critical flux were introduced in the work of Kwon et al. (Kwon et al., 2000); one was based on mass balance and the other one was defined on the basis of

the increase of transmembrane pressure (TMP). The critical flux based on mass balance was calculated from the rate of particle deposition at a certain permeate flux. Below the critical flux, there will be no particle deposition onto the membranes. The critical flux based on the TMP increase is the flux below which membrane fouling does not occur. The critical flux based on both definitions was evaluated from experiments.

The estimated results of our simulation show good agreement with the experimental results obtained by Kwon et al. (Kwon et al., 2000) for particles greater than $0.3 \mu m$. The critical fluxes predicted from our simulation are slightly lower than these obtained from the experiments based on the mass balance method, which can be explained in terms of inter-particle interactions. The ionic strength used in their experiments ranges from $O(10^{-5} - 10^{-3})M$, where colloidal particles are usually repulsive if their zeta potential is of an order of $O(10) mV$ in magnitude. Repulsive interaction among particles mitigates particle deposition, attenuates structural bisection, i.e., concentration polarization, and hence reduces values of order parameter. In other words, stronger repulsion between particles allows higher critical flux.

The goal of the current study is to delineate a consistent baseline of the critical flux using the non-interacting hard spheres undergoing only Brownian and shear-induced diffusion, i.e., pure equilibrium thermodynamics and non-equilibrium hydrodynamic

origins, respectively (Kim and Liu, 2007). From equation (3.10), without shear rate, the critical flux decreases when the particle size increases since larger particles will undergo stronger hydrodynamic drag forces toward the membrane surface. On the other hand, stronger shear enhances back diffusion of larger particles from the membrane surface to the bulk phase even when the Brownian diffusion is negligible. Figure 4.6 indicates that the critical flux of repulsive particles is higher than that of hard spheres with a size greater than $O(10^{-1}) \mu m$ and shear rate of $O(10^3)/sec$. Comparison of the critical flux measured indicates that the critical flux estimated from TMP method is always higher than that obtained from the mass balance method. This implies two different important stages in the critical flux determination in terms of particle distribution and deposition.

The critical flux determined from the mass balance method is close to our MC simulation, which may be due to both methods dealing with concentration polarization, i.e., spatial deviation of particle distribution away from the uniform configuration as the main criteria to determine the critical flux. The highest flux that initiates particle deposition in experiments corresponds to the flux that makes a transition of $d\psi / dv_w$ from the rapid linear decrease to the indifferent variation, as shown in Figure 4.5. The difference between experimental observations of the critical flux based on mass balance and our MC simulations are attributed to the interaction among particles, which is

considered to be repulsive due to the low ionic strength, $IS = 10^{-5} M$, of the feed solution of latex particles. In this case, both methods represent a steady state near which the initial, noticeable concentration polarization occurs with spatial bias of the particle distribution along the direction normal to the membrane surface. Therefore, the hydrodynamics (i.e., convective drag force) and thermodynamics (i.e., Brownian and shear-induced diffusion) are balanced. In this light, the critical flux estimated by TMP method indicates a thermodynamic state in which diffusion is readily suppressed by permeation. Due to the unceasing increase in TMP, the critical flux of the TMP method may possibly indicate another transition from quasi-equilibrium to pure irreversible (non-equilibrium) thermodynamic state, which is out of the scope of the current study.

CHAPTER 5. CONCLUSIONS

A large-scale Monte Carlo simulation method based on parallel computation via message passing interface (MPI) of crossflow membrane filtration for removal of particulate materials was developed to investigate the dynamic particle structures associated to the critical flux. Dominant mechanisms of particle transport, including Brownian and shear-induced diffusion, are unified to derive an effective hydrodynamic force. The force acting on each hard sphere includes gravitational, buoyant, and hydrodynamic drag forces in the direction normal to the membrane surface. The transition probability consists of tangential and normal biases, which are based on the axial convection and the hydrodynamic drag force, respectively.

In the Monte Carlo simulations, the variance of the particle distribution along the direction normal to the membrane surface is proposed to be an order parameter of the phase transition. The second order derivative of this order parameter is used to estimate the critical flux. Estimated critical fluxes are very close to experimental results measured using the mass balance method. Effects of shear rate and particle size on the critical flux

are investigated using this model, which determines a baseline by showing that repulsive particles lead to higher critical flux compared to hard spheres. In the light, this large-scale MC simulation is proven to be rigorous and effective in investigating the membrane fouling phenomena on a microscopic scale, and therefore, it is capable of providing optimal operational parameters, i.e., critical flux, for colloidal suspensions without strong inter-particle interactions.

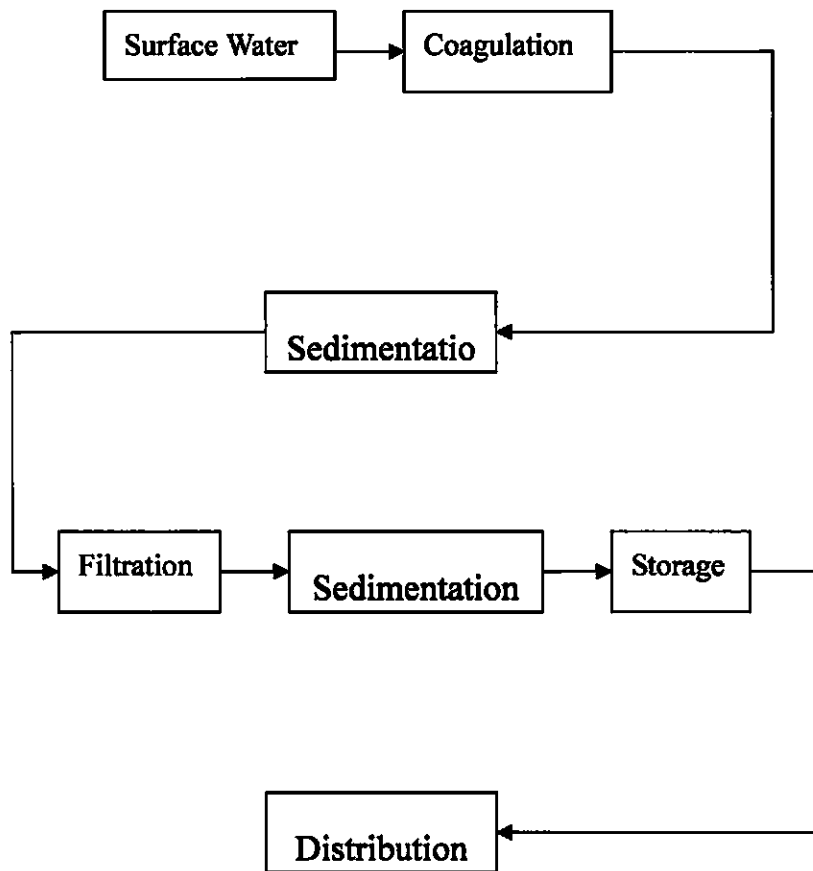


Figure 1.1 Diagram for a typical water treatment plant

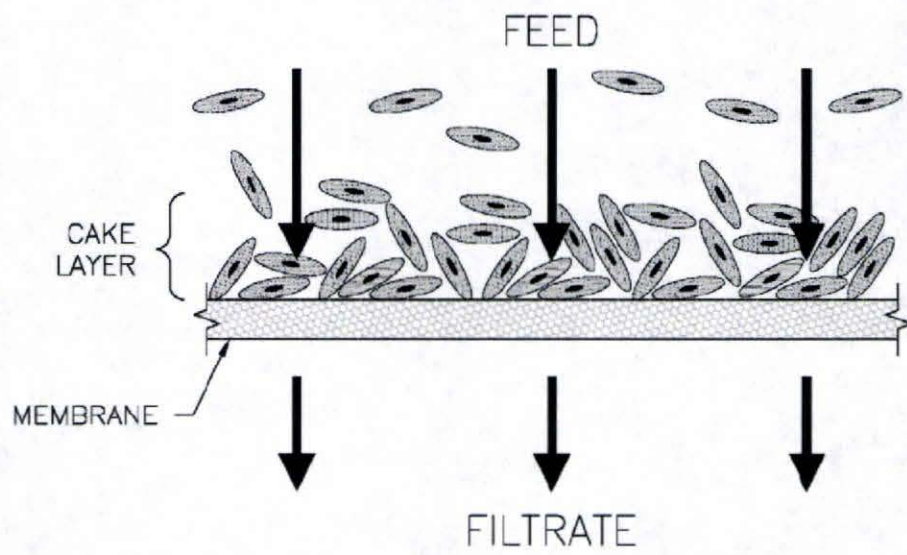


Figure 1.2 Conceptual illustration of dead-end filtration (EPA, 2005)

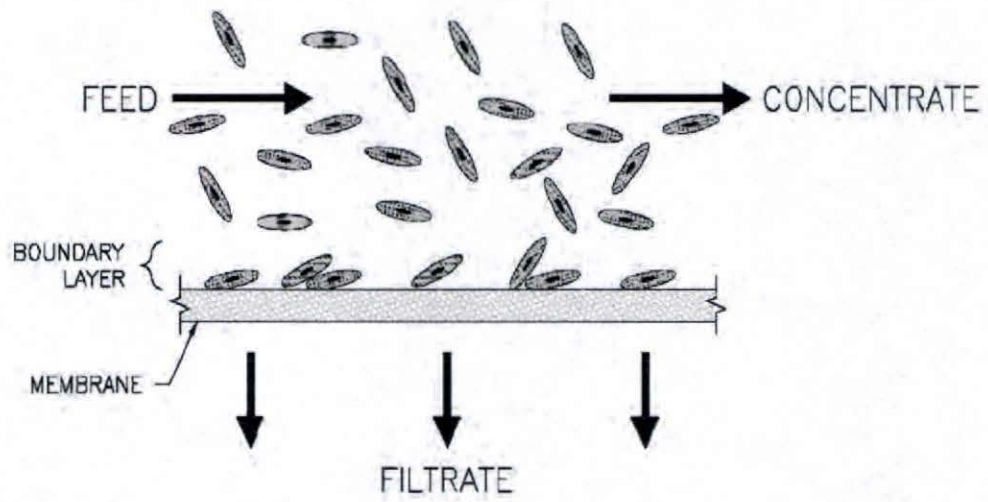


Figure 1.3 Conceptual illustration of crossflow filtration (EPA, 2005)

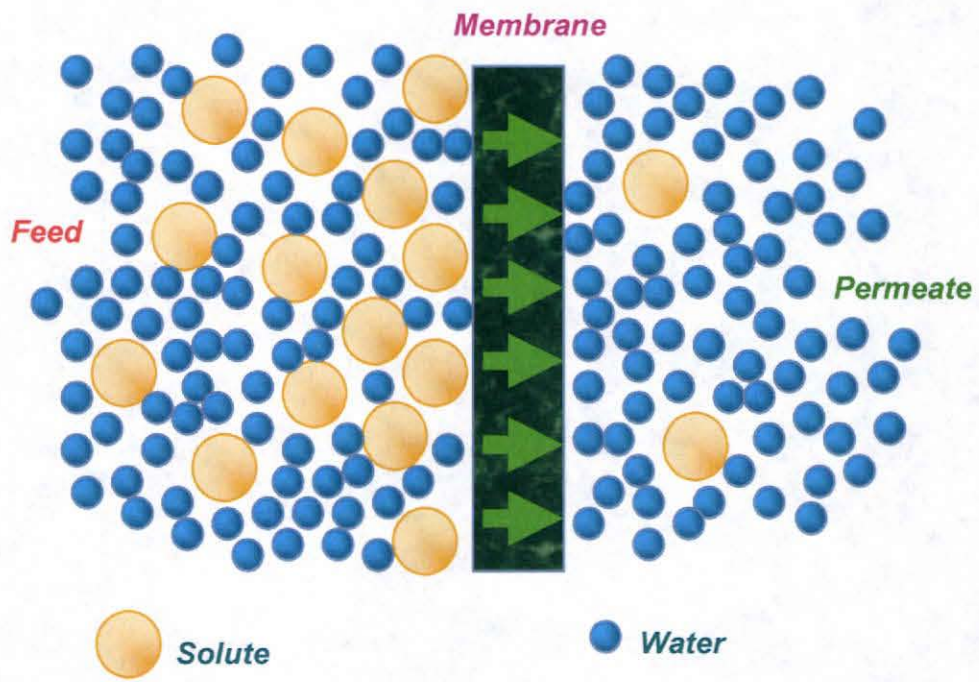


Figure 2.1 Diagram of membrane filtration process

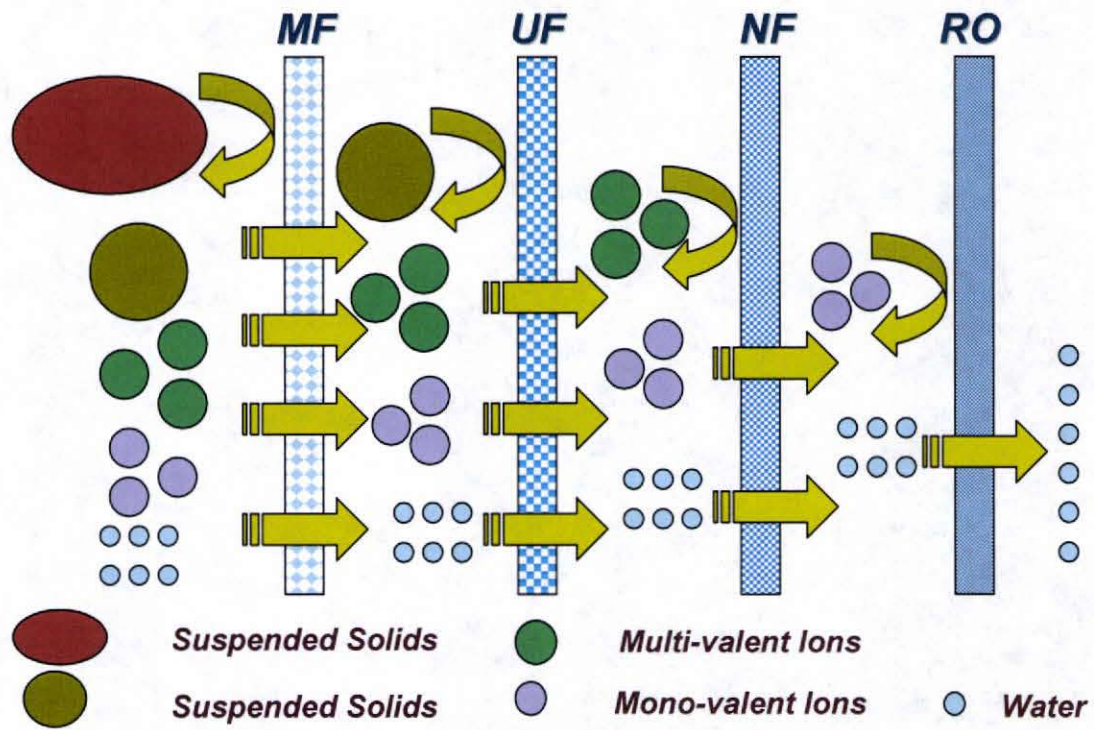


Figure 2.2 Diagram of membrane filtration processes of Microfiltration (MF), Ultrafiltration (UF), Nanofiltration (NF) and Reverse Osmosis (RO)

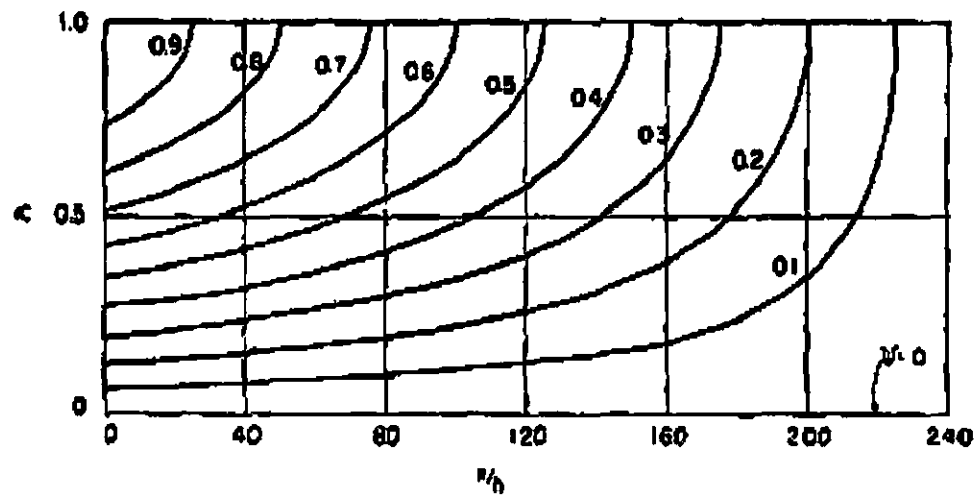


Figure 3.1 Flow lines in the upper half of membrane channel (Berman, 1953)

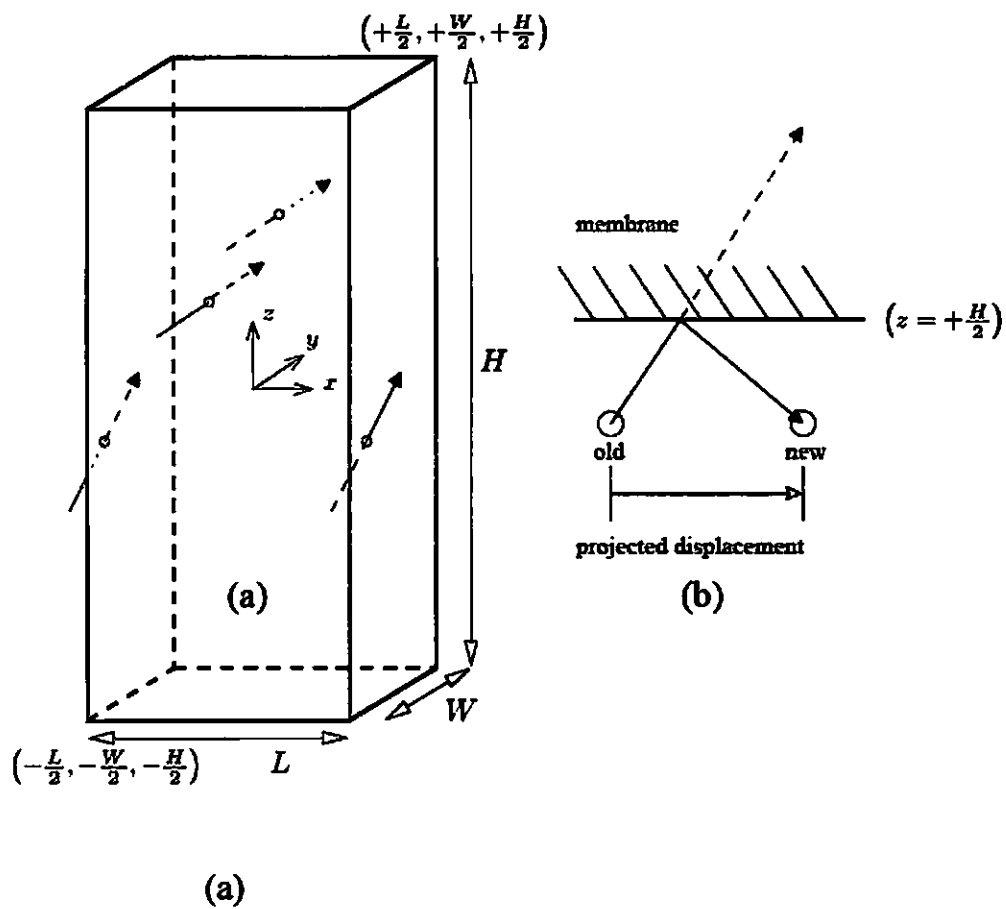


Figure 3.2 The simulation box as a representative volume.(a) Periodic boundary conditions in x - and y -directions.(b) Reflecting boundary condition in z -direction.

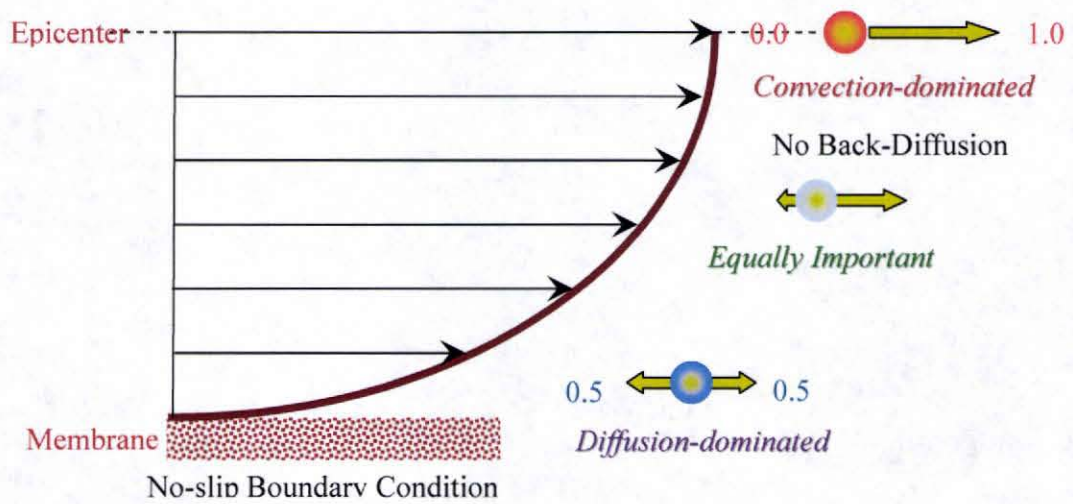


Figure 3.3 Dominant transport mechanisms at different locations within the membrane channel: the axial bias stemming from the flow profile

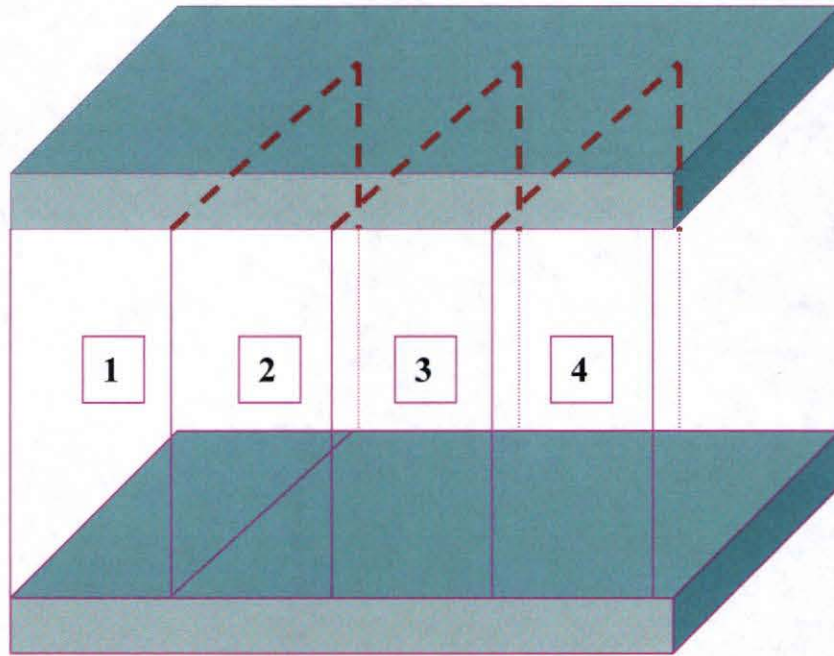


Figure 3.4 Domain decomposition among four processors along x -direction. The number on each box refers to the identification of the processor that is responsible for the calculation of that domain.

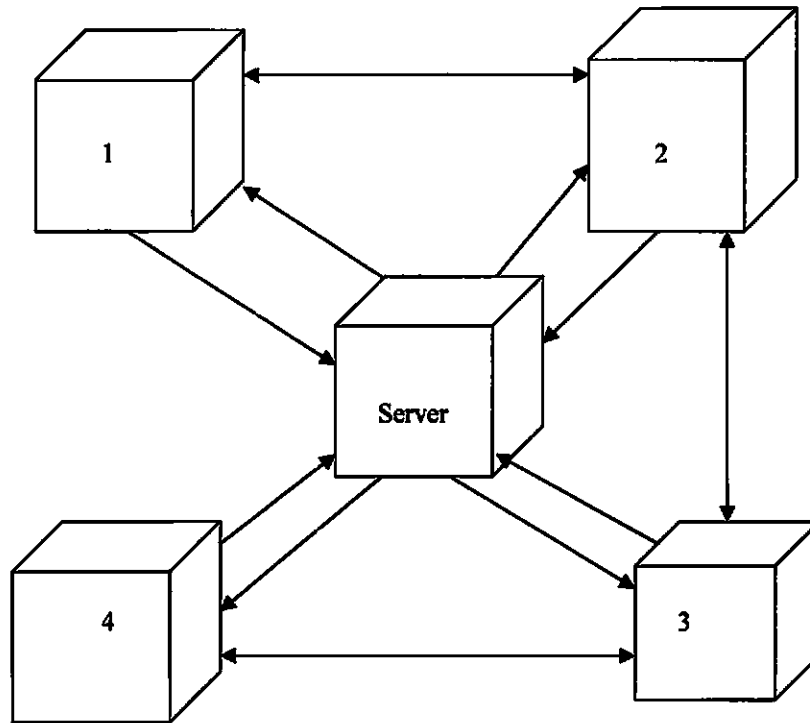


Figure 3.5 Diagram of master-slave parallel algorithm and MPI as shown in Figure 3.4.

After the calculation, slave nodes send data to the server, in the mean time, the server receives data from slaves. After reorganizing the data, the server re-decompose the task and send data to slaves, in the mean time, slaves receive data from the server. The neighbor slaves exchange data via MPI.

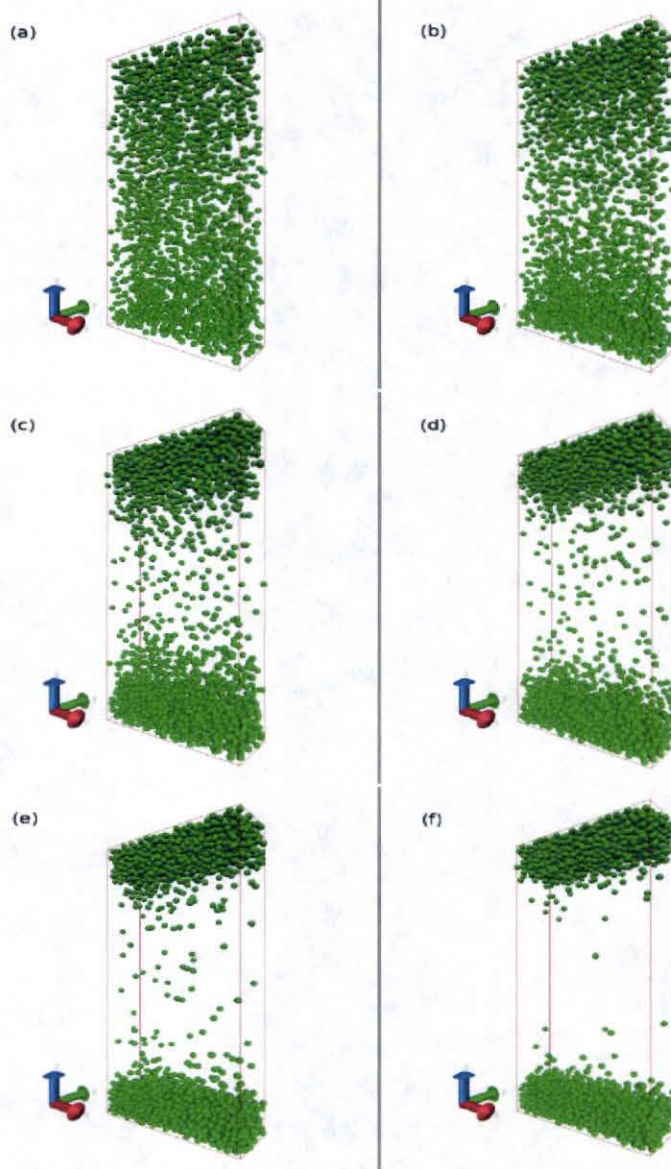


Figure 4.1 Canonical MC simulations with the number of particles $N_p = 2100$, particle radius $a = 0.1 \mu m$, mass density $\rho_p = \rho_f$, and shear rate $\dot{\gamma} = 10^3 \text{ sec}^{-1}$. The permeate flux v_w of simulations are (a) $0 \mu m$, (b) $1 \mu m$, (c) $5 \mu m$, (d) $10 \mu m$, (e) $20 \mu m$, and (f) $30 \mu m$.

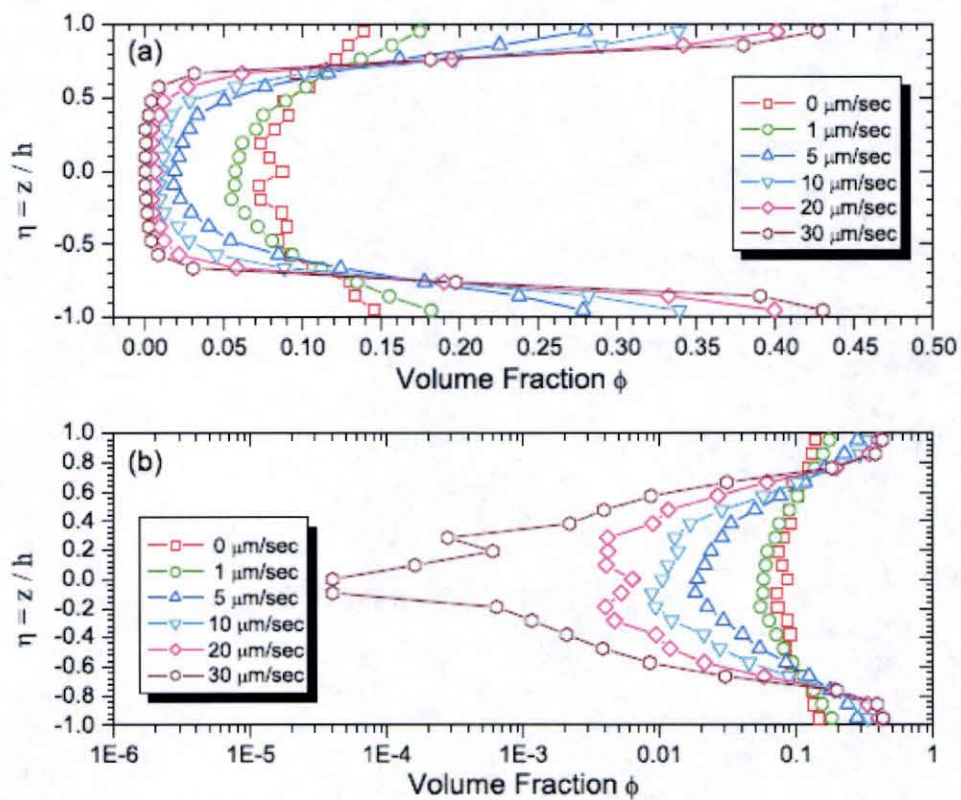


Figure 4.2 Profiles of particle volume fraction in the normal direction with various permeate fluxes with (a) linear and (b) common-log scales of volume fraction. Particle radius is $0.1 \mu\text{m}$, and shear rate is 1000sec^{-1} .

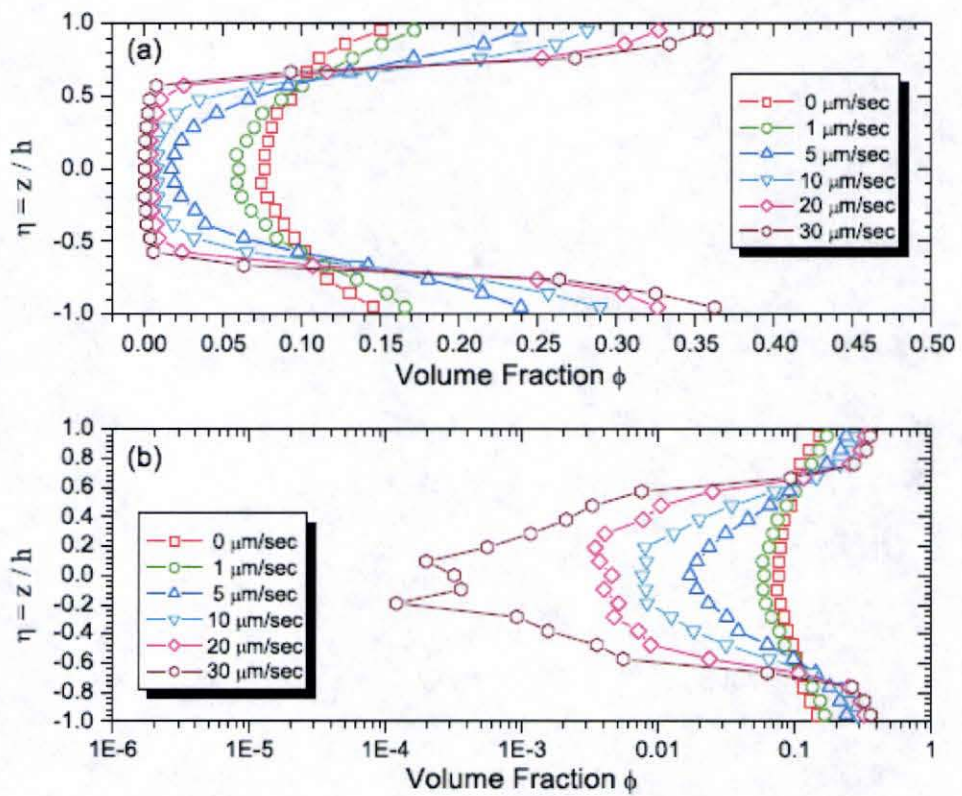


Figure 4.3 Profiles of particle volume fraction in the normal direction with various permeate flux with (a) linear and (b) common-log scales of volume fraction. Particle radius is $0.1 \mu\text{m}$, and shear rate is 5000sec^{-1} .

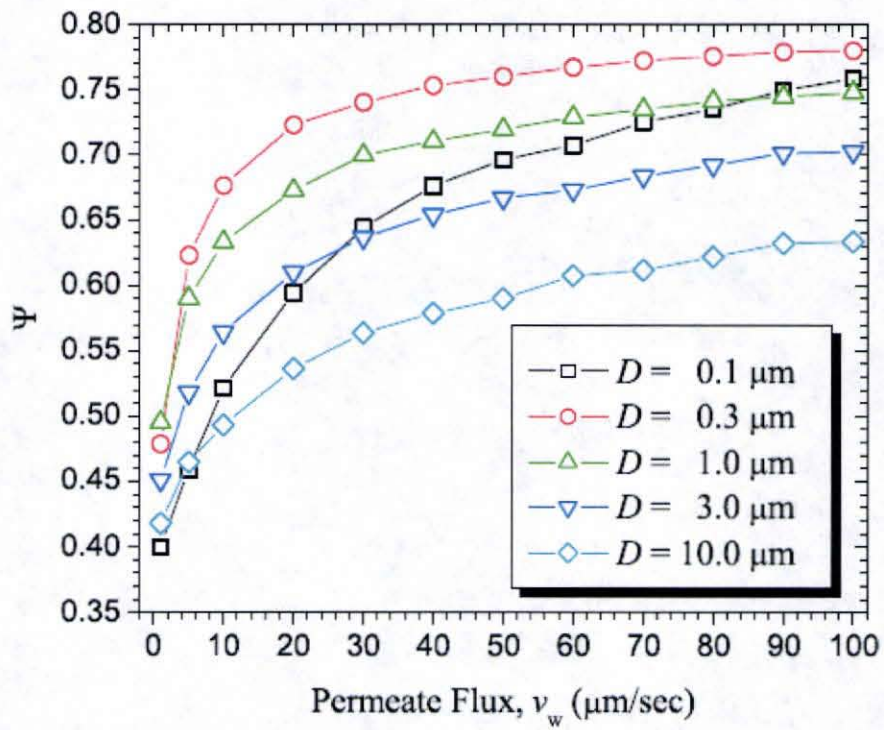


Figure 4.4 The order parameter defined as Eq. (4.1) versus the permeate flux. The order parameter increases with v_w and decreases with the particle diameter (excluding $D=0.1 \mu\text{m}$ case). The shear rate used for these simulations is $\dot{\gamma}_0 = 3.33 \times 10^3 \text{ sec}^{-1}$.

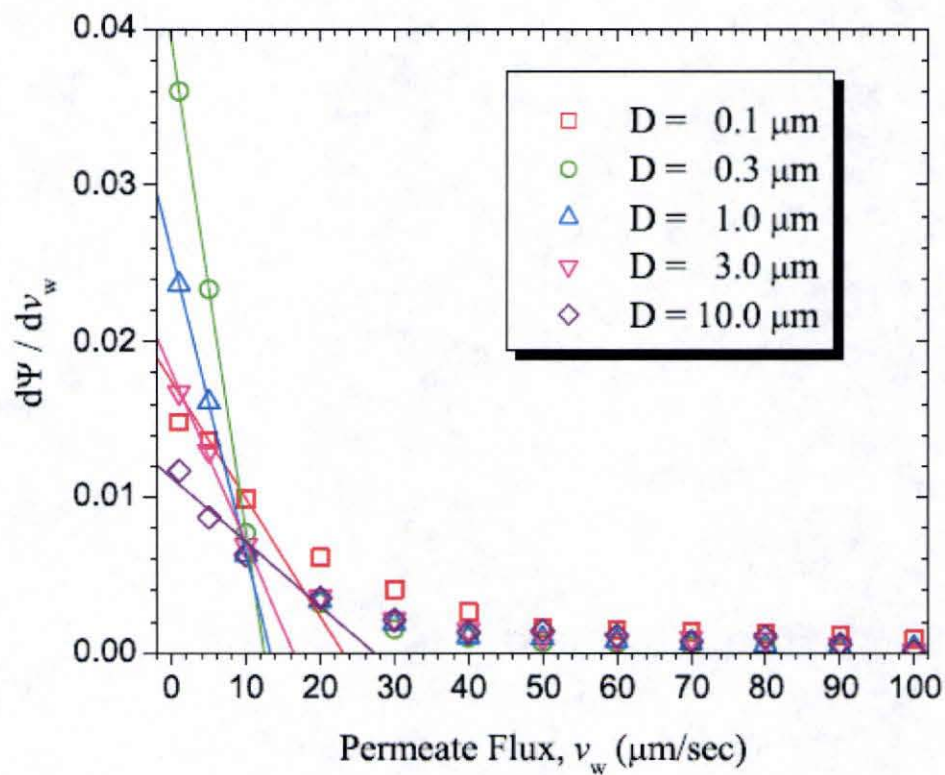


Figure 4.5 The derivative of the order parameter with respect to the permeate flux, obtained from Fig 4.4. Each arrow line indicates the linear regression using the first three data points from $v_w = 0$. Abscissas of the arrows (i.e., x -intercepts of regressed lines) points out critical fluxes based on the asymptotic discontinuity of the order parameter.

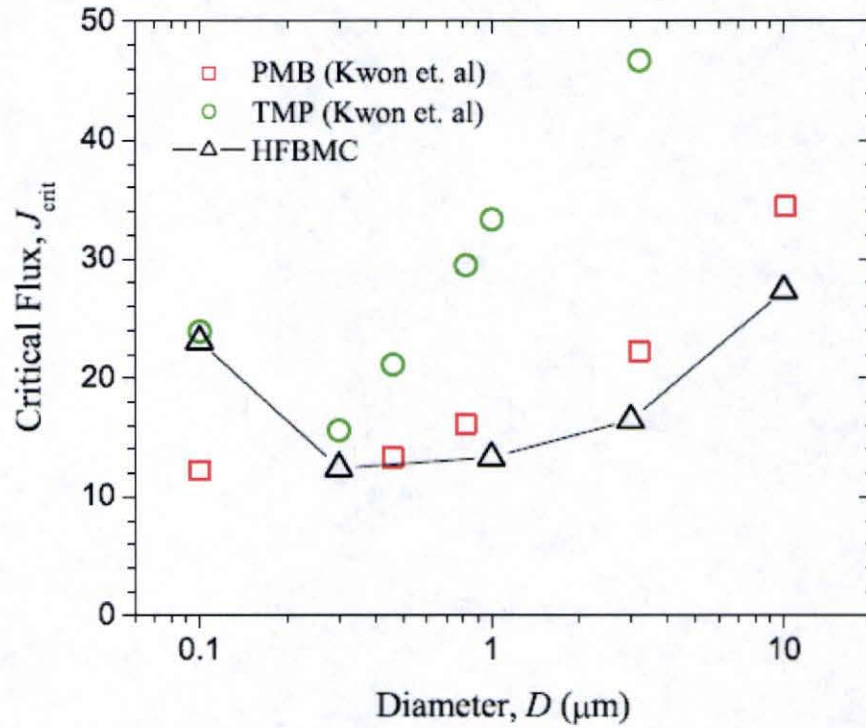


Figure 4.6 Comparison of critical fluxes of our model and experimental observation by Kwon et al. (Kwon et al., 2000) using particle mass balance (MB) and transmembrane pressure (TMP) methods. Operation conditions are as follows: crossflow $\bar{u} = 0.2\text{m/sec}$, ionic strength $IS = 10^{-5}M$, temperature $T = 25^{\circ}C$, membrane length $\bar{l} = 60\text{mm}$, width $\bar{w} = 6\text{mm}$, and half height $h = 18\text{mm}$. The estimated value of the shear rate is $\gamma_0 = 3.33 \times 10^3 \text{sec}^{-1}$.

REFERENCES

- Allen M.P., Brownian dynamics simulation of a chemical reaction in solution, *Molecular Physics*, 40 (1980), 1073-1087.
- Allen M.P. and D.J. Tildesley, *Computer simulation of liquids*, Oxford Clarendon Press, Oxford, UK, 1987.
- American Water Works Association Research Foundation, *Water Treatment Membrane Processes*, McGraw-Hill, New York, 1996.
- Bacchin P., P. Aimar, and V. Sanchez, Model for colloidal fouling of membranes, *American Institute of Chemical Engineer Journal*, 41 (1995), 368-376.
- Bacchin P., M. Meireles, and P. Aimar, Modeling of filtration: from the polarized layer to deposit formation and compaction, *Desalination*, 145 (2002), 139-146.
- Bacchin P., P. Aimar. and R.W. Field, Critical and sustainable fluxes: Theory, experiments and applications, *Journal of Membrane Science*, 281 (2006), 42-69.
- Bacchin P., B Espinase, Y. Bessiere, D.F. Fletcher and P. Aimar, numerical simulation of colloidal dispersion filtration: description of critical flux and comparison with experimental results, *Desalination*, 192 (2006), 74-81.
- Barger M. and R.P. Carnahan, Fouling prediction in reverse osmosis processes, *Desalination*, 83 (1991), 3-33.

- Barrat J.L. and J.P. Hansen, Basic concepts for simple and complex liquids, Cambridge University Press, New York, 2003.
- Belfort G., Fluid mechanics and cross-flow filtration in H.S. Muralidhara (Ed.), Advances in Solid-Liquid Separation, Battelle Press, Columbus, OH, 1986, Chap.7.
- Belfort G., R.H. Davis and A.L. Zydney, The behavior of suspensions and macromolecular solutions in crossflow microfiltration, Journal of Membrane Science, 96 (1994), 1-58.
- Bergman, R.A., Overview of membrane filtration for municipal water treatment. AWWA membrane conference proceedings March, 1999.
- Berman A.S., Laminar flow in channels with porous walls, Journal of Applied Physics 24 (1953), 1232-1235.
- Berman A.S., Laminar flow in channels with porous walls, Journal of Applied Physics 24 (1953) 1232-1235.
- Bowen and Jenner, Recovery of critical acid from fermentation beer using supported-liquid membranes, Advances in Colloid and Interface Science, 56 (1995), 141-200.
- Bowen W.R., T.A. Doneva and H.B. Yin, Separation of humic acid from a model surface water with PSU/SPEEK blend UF/NF membranes, Journal of Membrane Science, 206 (2002), 417-429.
- Bruggen B.V.D., C. Vandecasteele, T.V. Gestel, W. Doyen, R. Leysen, A review of pressure-driven membrane processes in wastewater treatment and drinking water

- production. *Environmental Progress*, 22 (2003), 46-59.
- Chen J.C. and A.S. Kim, Review of Brownian dynamics, molecular dynamics and Monte Carlo modeling of colloidal systems, *Advances in Colloid and Interface Science*, 112 (2004) 159-173.
- Chen J.C. M. Elimelech, and A.S. Kim, Monte Carlo simulation of colloidal membrane filtration: model development with application to characterization of colloid phase transition, *Journal of Membrane Science*, 255 (2005), 291-305.
- Chen J.C. and A.S. Kim, Monte Carlo simulation of colloidal membrane filtration: principal issues for modeling, *Advances in Colloid and Interface Science*, 119 (2006), 35-53.
- Davis, R. H. and D.T. Leighton, Shear-induced transport of a particle layer along a porous wall, *Chemical Engineering Science*, 42 (1987), 217-234.
- Davis, R.H. and Sherwood, A similarity solution for steady-state cross-flow microfiltration, *Chemical Engineering Science*, 45 (1990), 3203-3209.
- Duclos-Orsello C., W. Li, and C.C. Ho, A three mechanism model to describe fouling of microfiltration membranes, *Journal of Membrane Science*, 280 (2006), 856-866.
- Eckstein E.C., D.G. Bailey, and A.H. Shapiro, Self-diffusion of particles in shear flow of a suspension, *Journal of Fluid Mechanics*, 79 (1977), 191-208.
- Ermark, D.L. A computer simulation of charged particles in solution. I. Technique and equilibrium properties, *Journal of Chemical Physics*, 62 (1975), 4189 – 4196.
- Fane A.G. and C.J.D. Fell, A review of fouling and fouling control in ultrafiltration,

- Desalination, 62 (1987) 117-136.
- Field R.W., D. Wu, J.A. Howell and .B. Gupta, Critical flux concept for microfiltration fouling, *Journal of Membrane Science*, 100 (1995), 259-272.
- Fimbres-Weihs G.A. and D.E. Wiley, Numerical study of mass transfer in three-dimensional spacer-filled narrow channels with steady flow, *Journal of Membrane Science*, 306 (2007), 228-243.
- Flora J.R.V., Stochastic approach to modeling surface fouling of ultrafiltration membranes, *Journal of Membrane Science*, 76 (1993), 85-88.
- Gesan-Guiziu G., R.J. Wakeman, and G. Daufin, Stability of latexcrossflow filtration: cake properties and critical conditions of deposition, *Chemical Engineering Journal*, Vol. 85 (2002), 27-34.
- Ghidossi R., D. Veyret and P. Moulin, Computational fluid dynamics applied to membranes: State of the art and oportuities, *Chemical Engineering Process*, 45 (2006), 437-454.
- Hansen J.P. and I.R. McDonald, *Theory of simple liquids*, Academic Press, London, 1976.
- Happel J., Viscous flow in multiparticles systems: slow motion of fluids relative to beds of spherical particles, *American Institute of Chemical Engineer Journal*, (1958), 197-207.
- Ho C.C. and A.L. Zydney, Transmembrane pressure profiles during constant flux

- microfiltration of bovine serum albumin, *Journal of Membrane Science*, 209 (2002), 363-377.
- Howell J.A., Sub-critical flux operation of microfiltration, *Journal of Membrane Science*, 107 (1995), 165-171.
- Kanani D.M. and R. Ghosh, A constant flux based mathematical model for predicting permeate flux decline in constant pressure protein ultrafiltration, *Journal of Membrane Science*, 290 (2007), 207-215.
- Kavanaugh M. C. and J. O. Leckie, *Particulates in water*, Stanford University, 1980.
- Khulbe K C, Matsuura T, Lamarche G and Lamarche A-M, X-ray diffraction analysis of dense PPO membranes, *Journal of Membrane Science*, 170(2000), 81-89.
- Kim A.S., S. Bhattacharjee, and M. Elimelech, Shear-induced reorganization of deformable molecular assemblages: Monte Carlo studies, *Langmuir*, 17 (2001), 552-561.
- Kim A.S. and E.M.V. Hoek, Cake structure in dead-end membrane filtration: Monte Carlo simulation, *Environmental Engineering Science*, 19 (2002) 373-386.
- Kim A.S. and R. Yuan, A new model for calculating specific resistance of aggregated colloidal cake layers in membrane filtration processes, *Journal of Membrane Science*, 249 (2005), 89-101.
- Kim A.S. and Y. Liu, Irreversible chemical potential and shear-induced diffusion in crossflow filtration, *Industrial & Engineering Chemical Fundamentals*, submitted.
- Kim K.J., A.G. Fane and C.J.D. Fell, The performance of ultrafiltration membranes

pretreated by polymers, *Desalination*, 70 (1988), 229-249.

Kleinstreuer C. and G. Belfort, Mathematical modeling of fluid flow and solute distribution in pressure-driven membrane modules, in G. Belfort (Ed.), *Synthetic Membrane Processes: Fundamentals and Water Applications*, Academic Press, New York, NY, 1984, Chap.5.

Kozinski A.A. and E.N. Lightfoot, protein ultrafiltration: A general example of boundary layer filtration, *American Institute of Chemical Engineer Journal*, 18 (1972), 1030-1040.

Kramer P.W., Y.S. Yeh and H. Yasuda, Low temperature plasma for the preparation of separation membranes, *Journal of Membrane Science*, 46 (1989), 1-28.

Kwon, D. Y., S. Vigneswaran, A. G. Fane, R. Ben Aim, Experimental determination of critical flux in cross-flow microfiltration, *Separation and Purification Technology*, 19 (2000), 169-181.

Leighton D. and A. Acrivos, Viscous resuspension, *Chemical Engineering Science*, 41(1986), 1377-1384.

Leighton D. and A. Acrivos, Measurement of the shear induced coefficient of self-diffusion in concentration suspensions of spheres, *Journal of Fluid Mechanics* 177 (1987), 109-131.

Leighton D. and A. Acrivos, The shear-induced migration of particles in concentrated suspensions, *Journal of Fluid Mechanics* 181 (1987), 415-439.

Li H., A.G. Fane, H.G.L. Coster and S. Vigneswaran, Direct observation of particle

- deposition on the membrane surface during crossflow microfiltration, *Journal of Membrane Science*, 149 (1998), 83-97.
- Li H., A.G. Fane, H.G.L. Coster, and S. Vigneswaran, An assessment of depolarization models of crossflow microfiltration by direct observation through the membrane, *Journal of Membrane Science*, 172 (2000), 135-147.
- Manousiouthakis V.I. and M.W. Deem, Strict detailed balance is unnecessary in Monte Carlo simulation, *Journal of Chemical Physics*, 110 (1999), 2753-2756.
- Manttari M. and M. Nystrom, critical flux in NF of high molar mass polysaccharides and effluents from the paper industry, *Journal of Membrane Science*, 170 (2000), 257-273.
- Metropolis N., A.W. Rosenbluth, M.N. Rosenbluth, A.H. Teller, and E.J. Teller, Equation of state calculations by fast computing machines, *Chemical Physics*, 21 (1953), 1087-1092.
- Miclent S. and H. Carrere, Clarification of lactic acid fermentation broths, *Separation and Purification Technology*, 22-23 (2001), p393-401.
- Milisic V. and Ben Aim, R., Developing a better understanding of crossflow microfiltration, *Filtration & Separation Technology*, 1 (1986), 28-30.
- Mulder M., *Basic Principles of Membrane Technology*. Kluwer Academic Publishers, Boston, MA, 1996.
- Nystrom N. and P. Jarvinen, Modification of polysulfone ultrafiltration membranes with UV irradiation and hydrophilicity increasing agents, *Journal of Membrane Science*,

60 (1991), 275-296.

Parel H.W., Microbial attachment to particles in marine and freshwater ecosystems, *Aquatic Microbial Ecology*, 2 (1975), 73-79.

Porter M.C., Concentration polarization with membrane ultrafiltration, *Industrial & Engineering Chemistry Product Research Development*, 11 (1972), 234-248.

Rahimi M., S.S. Madaeni and K. Abbasi. CFD modeling of permeate flux in cross-flow microfiltration membrane, *Journal of Membrane Science*, 255 (2005), 23-31.

Ranade V.V. and A. Kumar, fluid dynamics of spacer filled rectangular and curvilinear channels, *Journal of Membrane Science*, 271 (2006), 1-15.

Romero C.A. and R.H. Davis, Transient model of cross-flow microfiltration, *Chemical Engineering Science*, 45 (1990), 13-25.

Santos J.L.C., V. Geraldes, S. Velizarov and J.G. Crespo, Investigation of flow patterns and mass transfer in membrane module channels filled with flow-aligned spacers using computational fluid dynamics (CFD), *Journal of Membrane Science*, 305 (2007), 103-117.

Schwinge J., D.E. Wiley and D.F. Fletcher, A CFD study of unsteady flow spacer-filled channels for spiral-wound membrane modules, *Desalination*, 146 (2002), 195-201.

Sethi S. and M. R. Wiesner, Modeling of transient permeate flux in cross-flow membrane filtration incorporating multiple particle transport mechanisms, *Journal of Membrane Science*, 136 (1997), 191-205.

- Sierou A. and J.F. Barady, Shear-induced self-diffusion in non-colloidal suspensions, *Journal of Fluid Mechanics*, 506 (2004), 285-314.
- Smith P.J., S. Vigneswaran, H.H. Ngo, R. Ben-Aim and H. Nguyen, Design of a generic control system for optimizing back flush durations in a submerged membrane hybrid reactor, *Journal of Membrane Science*, 255 (2005), 99-106.
- Smith P.J., S. Vigneswaran, H.H. Ngo, R. Ben-Aim and H. Nguyen, A new approach to backwash initiation in membrane systems, *Journal of Membrane Science*, 278 (2006), 381-389.
- Soppe W., "Computer Simulation of Random Packings of Hard Spheres," *Powder Tech.*, 62 (1990), 189-196.
- Takaba H., A. Yamamoto and S. Nakao, Modeling of methane permeation through a defective region in MFI-type zeolite membranes, *Desalination*, 192 (2006), 82-90.
- Tung K.L., K.T. Lu, R.C. Ruaan and J.Y. Lai, MD and MC simulations analyses on the effect of solvent types on accessible free volume and gas sorption in PMMA membranes, *Desalination*, 192 (2006), 391-400.
- Van Gunsteren W.F. and H.J.C. Berendsen, Algorithms for macromolecular dynamics and constraint dynamics, *Molecular Physics*, 34 (1977), 1311-1327.
- Verlet L., Computer 'experiments' on classical fluids, *Physical Review*, 159 (1967), 98-103.
- Vilker V.L., C.K. Colton, and K.A. Smith, Concentration polarization in protein ultrafiltration. Part I: An optical shadowgraph technique for measuring

concentration profiles near a solution-membrane interface, American Institute of Chemical Engineer Journal, 27 (1981), 632-636.

Wu D.X., J.A. Howell, and R.W. Field, Critical flux measurement for model colloids, Journal of Membrane Science, 152 (1999), 89-98.

Zeman L.J. and A.L. Zydney (1996), Microfiltration and Ultrafiltration: principles and applications, Marcel Dekker Inc.

Zhang Y.P., A.G. Fane and A.W.K. Law, Critical flux and particle deposition of bidisperse suspensions during crossflow microfiltration, Journal of Membrane Science, 282 (2006), 189-197.

Zydney A.L. and Colton C.K., A concentration polarization model for the filtrate flux in cross-flow microfiltration of particulate suspensions, Chem. Eng. Comm., 47 (1986) 1-21.